Published in final edited form as:

Nat Cell Biol. 2018 June ; 20(6): 688–698. doi:10.1038/s41556-018-0106-3.

Spectrin is a mechanoresponsive protein shaping fusogenic synapse architecture during myoblast fusion

Rui Duan[1,#,†], **Ji Hoon Kim**[1,#], **Khurts Shilagardi**[1,#], **Eric Schiffhauer**[2], **Donghoon M. Lee**[3], **Sungmin Son**[4], **Shuo Li**[1], **Claire Thomas**[5], **Tianzhi Luo**[6], **Daniel A. Fletcher**[4], **Douglas N. Robinson**[2], and **Elizabeth H. Chen**[1,3]

[1]Department of Molecular Biology and Genetics, Baltimore, MD 21205, USA

[2]Department of Cell Biology, Johns Hopkins University School of Medicine, Baltimore, MD 21205, USA

[3]Department of Molecular Biology, UT Southwestern Medical Center, Dallas, TX 75390, USA

[4]Department of Bioengineering, University of California, Berkeley, Berkeley, CA 94720, USA

[5]Departments of Biology and of Biochemistry and Molecular Biology, Penn State University, University Park, PA 16802

[6]Department of Modern Mechanics, University of Science and Technology of China, Hefei, China

Abstract

Spectrin is a membrane skeletal protein best known for its structural role in maintaining cell shape and protecting cells from mechanical damage. Here, we report that α/β_H-spectrin (β_H is also called karst) dynamically accumulates and dissolves at the fusogenic synapse between fusing *Drosophila* muscle cells, where an attacking fusion partner invades its receiving partner with actin-propelled protrusions to promote cell fusion. Using genetics, cell biology, biophysics and mathematical modeling, we demonstrate that spectrin exhibits a mechanosensitive accumulation in response to shear deformation, which is highly elevated at the fusogenic synapse. The transiently accumulated spectrin network functions as a cellular fence to restrict the diffusion of cell adhesion molecules and a cellular sieve to constrict the invasive protrusions, thereby increasing the mechanical tension of the fusogenic synapse to promote cell membrane fusion. Our study reveals a

Correspondence and requests for materials should be addressed to E.H.C (Elizabeth.Chen@UTSouthwestern.edu).
[#]These authors contributed equally

Author Contributions

R.D. initiated the project. R.D., J.K., K.S. and E.H.C. planned the project, performed experiments in Figures 1, 2, 3, 5, 7, Supplementary Figures 1, 2, 4, 6 and Supplementary Videos 1, 2, 3, 4, 6, 7, 8, 9, and discussed the data. J.K. and E.H.C. collaborated with E.S. and D.N.R. on the MPA experiments in Figure 4a-e and Supplementary Figure 3, and with S.S. and D.A.F. on the AFM experiments in Figure 4k-l and Supplementary Video 5. D.H.L carried out the SIM experiments in Figure 6 and Supplementary Video 10. S.L. carried out the EM experiments in Figure 5h. T.L. developed the coarse-grained models in Figure 4f-j and Supplementary Figure 5. C.T. contributed spectrin constructs. R.D., J.K., K.S., D.M.L., E.S., T.L., D.N.R. and E.H.C. made the figures. J.K and E.H.C. wrote the paper. All authors commented on the manuscript.

[†]Present address: Laboratory of Regenerative Medicine in Sports Science, School of Sports Science, South China Normal University, Guangzhou, China

The authors declare no competing financial interests

function of spectrin as a mechanoresponsive protein and has general implications for understanding spectrin function in dynamic cellular processes.

The mechanical properties of cells are dynamically controlled in many cellular processes, such as cell division, fusion, migration, invasion, and shape change. Spectrin is best known as a membrane skeletal protein critical for maintaining cell shape and providing mechanical support for plasma membrane[1–3]. The functional unit of spectrin is a flexible, chain-like heterotetramer composed of two antiparallel heterodimers of α- and β-spectrin that interact head to head to form a tetramer[1–3]. While vertebrates have two α (αI and αII) and five β-spectrins (βI to V), invertebrates encode one α and two β-spectrins (β and β_{Heavy}). In erythrocytes and neurons, spectrins, together with actin, ankyrin and associated proteins, form either a static polygonal lattice structure[4–6] or an ordered periodic longitudinal array[7] underneath the plasma membrane to protect cells from mechanical damage[8]. Such a mechanoprotective function of spectrin is made possible by holding the spectrin network under constitutive tension[9]. However, in many cellular processes, mechanical tension is generated upon transient cell-cell interactions. How spectrins, which are expressed in most eukaryotic cells, respond to transient mechanical stimuli in dynamic cellular processes remains largely unknown.

Cell-cell fusion is a dynamic process that occurs in fertilization, immune response, bone resorption, placenta formation, and skeletal muscle development and regeneration[10, 11]. Studies in a variety of cell fusion events from *Drosophila* to mammals have demonstrated that cell fusion is an asymmetric process[12–17]. At the site of fusion, known as the fusogenic synapse, an attacking fusion partner invades its receiving fusion partner with actin-propelled membrane protrusions[12–14, 16, 17], whereas the receiving fusion partner mounts a myosin II (MyoII)-mediated mechanosensory response[14]. The pushing and resisting forces from the two fusion partners bring the two cell membranes into close proximity and put the fusogenic synapse under high mechanical tension to promote fusogen engagement and cell membrane merger[13, 14]. Although multiple long and narrow invasive protrusions from the attacking fusion partner are known to be required for cell-cell fusion[12, 13, 18, 19], it is unclear how these protrusions are spatially constricted and shaped in order to generate high mechanical tension at the fusogenic synapse.

RESULTS

α/β_H-spectrin is required for *Drosophila* myoblast fusion

In a deficiency screen for genes required for myoblast fusion, we uncovered *Df(3L)*1226. Genetic analyses of candidate genes within this deficiency led to the identification of *β_{heavy}-spectrin* (*β_H-spectrin*), also known as *karst* or *kst*[20, 21]. Zygotic null mutants of *α*- or *β_H-spectrin* exhibited minor myoblast fusion defects (Fig. 1ai-iv; 1b), likely due to maternal contribution. *α/β_H-spectrin* double mutant showed a severe fusion defect (Fig. 1av; 1b), suggesting that α/β_H-spectrin heterotetramer formation was significantly compromised when the concentrations of both α- and β_H-spectrin were low. The functional specificity of α/β_H-spectrin in myoblast fusion was demonstrated by a genetic rescue experiment, in which full-length β_H-spectrin expressed in all muscle cells rescued the fusion defect in *β_H-*

spectrin mutant (Fig. 1avii; 1b). In contrast, overexpressing dominant-negative β_H-spectrin (mini-β_H-spectrin, deleting 15 of the 29 spectrin repeats)[22] or β-spectrin containing 17 spectrin repeats[23] in muscle cells exacerbated the fusion defect of *β_H-spectrin* mutant (Fig. 1avi; 1b; Supplementary Fig. 1a), and caused a minor fusion defect in wild-type embryos (Supplementary Fig. 1a). Thus, both mini-β_H-spectrin and β-spectrin interfere with α/β_H-spectrin heterotetramer formation and disrupt the α/β_H-spectrin network. Moreover, β_H-spectrin expression specifically in the receiving fusion partners (muscle founder cells), but not in the attacking cells (fusion-competent myoblasts or FCMs), rescued the fusion defect (Fig. 1aviii and ix), demonstrating that α/β_H-spectrin functions specifically in founder cells.

α/β_H-spectrin enrichment at the fusogenic synapse in founder cells

To determine the subcellular localization of α/β_H-spectrin, we performed antibody-labeling experiments using anti-α- and β_H-spectrin in wild type (Fig. 1ci-ii), and anti-Flag and anti-GFP in two protein trap lines, *$kst^{MI03134}$* (Fig. 1ciii) and *$kst^{CPTI002266}$* (Fig. 1civ). Both α- and β_H-spectrin were enriched at the fusogenic synapse, largely co-localizing with Dumbfounded (Duf), an Ig domain-containing founder cell adhesion molecule (CAM)[24], and closely associating with the FCM-specific F-actin focus, part of an invasive podosome-like structure (PLS)[4]. In contrast, β-spectrin was not detected in muscle cells, despite its high expression in epithelial cells (Supplementary Fig. 1b). Ectopically expressed β-spectrin in muscle cells did not enrich at the fusogenic synapse as did α/β_H-spectrin and mini-β_H-spectrin (Fig. 1c; Supplementary Fig. 1e). In addition, two of the major accessory proteins known to stabilize spectrin-actin interactions, adducin[25] and protein 4.1[26, 27], were also absent at the fusogenic synapse (Supplementary Fig. 1c, d). An N-terminally tagged, functional β_H-spectrin (V5-β_H-spectrin) specifically expressed in founder cells, but not FCMs, was enriched at the fusogenic synapse (Fig. 1cv-vi), supporting the functional requirement for α/β_H-spectrin in founder cells.

Dynamic accumulation of α/β_H-spectrin at the fusogenic synapse

To investigate whether α/β_H-spectrin forms a stable membrane skeletal network at the fusogenic synapse, we performed live imaging experiments in *Drosophila* embryos. Surprisingly, instead of forming a static network, mCherry-β_H-spectrin exhibited dynamic accumulation and dissolution at the fusogenic synapse accompanying the appearance and disappearance of the FCM-specific F-actin focus (life span 6–30 min, average ~12 min[28]) (Fig. 2a, b; Supplementary Video 1). The amount of β_H-spectrin accumulation correlated with the density and invasiveness of the F-actin foci, with a higher accumulation in wild type (Fig. 2a, b; Supplementary Video 1) and an overall weaker accumulation in *dpak3* mutant, in which actin foci are loosely packed and less invasive[19] (Fig. 2c, d; Supplementary Video 2). Thus, spectrin forms a transient and dynamic structure that rapidly changes its density and morphology corresponding to the invasiveness of the PLS. The dynamic behavior of β_H-spectrin at the fusogenic synapse was confirmed by fluorescence recovery after photobleaching (FRAP). The fluorescence of photo-bleached mCherry-β_H-spectrin rapidly recovered with an average $T_{1/2}$ of 66 ± 35 sec, similar to that of the F-actin foci in FCMs (70 ± 18 sec)[12], and eventually reached 67 ± 14% of the pre-bleaching level (Fig. 2e and f; Supplementary Video 3). Thus, PLS invasion and α/β_H-spectrin accumulation were temporally coordinated and new α/β_H-spectrin heterotetramers were continuously recruited

to the fusogenic synapse in response to PLS invasion. Moreover, FRAP analysis of mCherry-β_H-spectrin expressed in epithelial cells also showed fluorescence recovery to a similar level, albeit at a slower rate, likely due to the different mechanical properties of the two cellular environment (Supplementary Fig. 2; Supplementary Video 4). Taken together, the dynamic behavior of β_H-spectrin is not restricted to muscle cells and is a general feature of this protein.

α/β_H-spectrin accumulates to the fusogenic synapse in the absence of chemical signaling

Given the correlation between spectrin accumulation and PLS invasiveness, we tested whether β_H-spectrin accumulation at the fusogenic synapse is triggered by the protrusive force from FCMs or recruited by the founder CAMs, Duf and its functionally redundant paralog Roughest (Rst)[24, 29]. Remarkably, β_H-spectrin still accumulated to fusogenic synapses in *duf,rst* double mutant expressing Duf lacking its entire intracellular domain (DufΔintra) (Fig. 3a; 3bi-ii; 3c), the latter of which does not transduce chemical signals but functions normally to attract the FCM-specific Ig domain-containing CAM, Sticks and stones (Sns)[30–32]. The overall weaker accumulation of β_H-spectrin in these mutant embryos corresponds to a partial rescue of myoblast fusion[33] (Fig. 3c). In contrast, Antisocial (Ants)/Rols7, a founder cell-specific adaptor protein that binds the intracellular domain of Duf[34–37], did not accumulate to the fusogenic synapse (Fig. 3bi-iii; 3c). Thus, β_H-spectrin accumulation in founder cells can be triggered by invasive forces from the PLS, independent of chemical signaling from CAMs. Furthermore, β_H-spectrin also accumulated to the fusogenic synapse in cultured *Drosophila* S2R+ cells induced to fuse by co-expressing Sns and a *C. elegans* fusogen Eff-1[13, 38]. Specifically, the F-actin foci in attacking cells were always associated with β_H-spectrin accumulation in receiving cells, despite the lack of endogenous Duf and Rst in these cells[13] (Fig. 3d).

α/β_H-spectrin exhibits mechanosensitive accumulation

To test directly whether β_H-spectrin exhibits mechanosensitive accumulation, we performed micropipette aspiration (MPA) assays, in which a pulling force is applied to *Drosophila* S2 cells by a micropipette. GFP-β_H-spectrin showed rapid mechanosensitive accumulation to the base area of the aspirated portion of the cell (Fig. 4a, d), in contrast to the previously demonstrated tip accumulation of the mechanosensory protein myosin II (MyoII)[14]. This effect was not due to an increased amount of membranous materials, F-actin or adaptor proteins at the base area, since an RFP-tagged PtdIns(4,5)P2-interacting pleckstrin homology (PH) domain[39], GFP-actin or Ants did not accumulate to this area (Fig. 4bi-ii, d; Supplementary Fig. 3ai, b). In addition, no accumulation was observed for GFP-β_H-spectrin-ΔC, which deleted a C-terminal fragment containing the tetramerization domain[40](Fig. 4biii, d; Supplementary Fig. 4a), or GFP-β_H-spectrin-ΔN, which deleted an N-terminal fragment containing the actin-binding domain[40] (Fig. 4biv, d; Supplementary Fig. 4a, b), suggesting that tetramerization and actin-binding activities are required for β_H-spectrin accumulation. α-spectrin only exhibited mechanosensitive accumulation when co-expressed with β_H-spectrin, but not expressed alone, in S2 cells (Supplementary Fig. 3ai-ii, b), consistent with the higher expression of endogenous β-spectrin than β_H-spectrin in these cells (FlyBase)[41], the former of which was not mechanosensitive demonstrated by MPA assays (Supplementary Fig. 3aiii, b). Notably, the mechanosensitive accumulation of β_H-spectrin is

time- and force-dependent, which increased linearly over time until reaching its peak level at 80–90 sec after the onset of aspiration (Supplementary Fig. 3c) and increased proportionally to applied pressure (Supplementary Fig. 3d). These results indicate that α/β_H-spectrin binding to the actin network depends on the number of binding sites at a given time rather than additional cooperative activity of the previously bound tetramers, and that the mechanical force applied to the cortical actin network leads to increased number of binding sites for the α/β_H-spectrin heterotetramers.

α/β_H-spectrin responds to shear deformation

It is intriguing that α/β_H-spectrin and MyoII show distinct patterns of mechanosensitive accumulation revealed by MPA. Previous coarse-grained modeling suggests that the tip of an aspirated cell corresponds to an area of maximal actin network dilation (or radial expansion), whereas the base area corresponds to maximal shear deformation (or shape change)[42]. MPA analyses suggest that MyoII is a mechanosensory protein for actin network dilation, whereas α/β_H-spectrin responds specifically to shear deformation. Consistent with the distinct areas of mechanosensitive accumulation of MyoII and spectrin, β_H-spectrin remained at the base area in cells treated with Y27632, a small molecule that decreases MyoII activity by inhibiting MyoII's upstream activator ROCK (compare Fig. 4ci and ii; Fig. 4d), and MyoII (RFP-Zip[14]) remained at the tip of β_H-spectrin knockdown cells (compare Fig. 4ci and iii; Fig. 4e). At late time points, weak β_H-spectrin accumulation was observed at the neck and tip areas of aspirated cells in a MyoII-dependent manner (Fig. 4a, 85s; Supplementary Fig. 3aiii), suggesting that MyoII-mediated cortical contraction at the tip may gradually create shear deformation along the aspirated portion of the cell.

The distinct domains of mechanosensitive accumulation of MyoII and spectrin induced by pulling forces prompted us to ask whether they exhibit a similar response to pushing forces. Course-grained modeling of cells invaded by protrusions with a 5-μm diameter predicted clear separation of dilation vs. shear domains along the invasive protrusion, with maximal dilation corresponding to the tip and maximal shear deformation to the base (Fig. 4f). However, when the invasive protrusions became narrower (~400 nm diameter), there was a gradual increase of shear deformation at the tip, where the dilation deformation remained largely the same (Fig. 4g-j). This model predicted that the mechanosensitive accumulations of β_H-spectrin and MyoII induced by narrow protrusions may no longer be clearly separated. To test this directly, we performed atomic force microscopy (AFM) experiments, in which a pushing force was applied to cells expressing GFP-β_H-spectrin and RFP-MyoII by a cantilever with a tip diameter of ~200 nm, mimicking the length scale of the invasion protrusions at a mature fusogenic synapse (Fig. 4k). When indented for 2–5 μm, β_H-spectrin and MyoII exhibited rapid and largely overlapping domains of accumulation to the indented area (Fig. 4l; Supplementary Video 5), consistent with the pattern of mechanosensitive response predicted by the course-grained model and the enrichment of both β_H-spectrin and MyoII at the fusogenic synapse in *Drosophila* embryos (Fig. 1c)[14].

α/β_H-spectrin restricts cell adhesion molecules at the fusogenic synapse

What are the biological functions of spectrin accumulation at the fusogenic synapse? In *α/β_H-spectrin* double mutant, the founder cell CAM Duf and its interacting protein Ants were

both dispersed at the fusogenic synapse, instead of forming a tight aggregate as in wild type (Fig. 5a, b). Time-lapse imaging revealed the dynamic dispersion of Duf in these embryos (Supplementary Video 6), compared to the tight Duf cluster associated with dense F-actin foci in wild type (Fig. 5c; Supplementary Video 7). Occasional Duf aggregates in mutant embryos gradually diffused over time, suggesting that α/β_H-spectrin is required for the maintenance, but not the initiation, of the Duf clusters (Fig. 5d; Supplementary Video 6).

Since Duf and Sns interact in trans[31], we tested whether Duf dispersal in founder cells of *α/β_H-spectrin* mutant affects Sns distribution in FCMs. Indeed, Sns was also dispersed at the fusogenic synapse in these embryos (Fig. 5e), and so did the actin nucleation-promoting factors (NPFs) and their interacting proteins, such as the WASP-interacting protein (WIP; also known as Solitary or Sltr), which is recruited by Sns to the fusogenic synapse[43, 44] (Fig. 5f). The diffusion of actin NPFs resulted in a fuzzy F-actin structure in the FCM (Fig. 5a, b, d, e, f), with an average fluorescence intensity of 61 ± 19 per focus on a 0–255 scale (n=35), compared to 170 ± 15 per focus (n=28) in wild type. The low intensity of F-actin indicates a low filament density, which generated stubby and closely abutting toe-like protrusions, instead of the long, narrow and well separated fingerlike protrusions in wild type (Fig. 5h)[12, 18, 19]. Thus, Duf restriction by α/β_H-spectrin in founder cells regulates Sns localization and the distribution of actin filaments at the fusogenic synapse in FCMs.

α/β_H-spectrin maintains Duf enrichment at the fusogenic synapse via biochemical interactions

To investigate how spectrin restricts Duf at the fusogenic synapse, we performed co-immunoprecipitation experiments using *Drosophila* embryos expressing Flag-β_H-spectrin and Duf-GFP in muscle cells. An antibody against Flag, but not a control antibody, co-precipitated α-spectrin and Duf-GFP, suggesting that the α/β_H-spectrin heterotetramers interact with Duf (Fig. 5i; Supplementary Fig. 5a). Moreover, DufΔintra, which can no longer interact with α/β_H-spectrin, appeared diffused at many fusogenic synapses in *duf,rst* mutant, similar to Duf diffusion in *α/β_H-spectrin* mutant (Fig. 5g). As a consequence, the F-actin foci that formed initially due to the trans-interactions between DufΔintra and Sns also gradually dispersed at the fusogenic synapse (Supplementary Video 8) as in *α/β_H-spectrin* mutant (Fig. 5a, b, d, e, f; Supplementary Video 7). Interestingly, time-lapse imaging revealed a gradual diffusion of accumulated β_H-spectrin in DufΔintra-expressing *duf,rst* mutant embryos (Supplementary Video 9), suggesting that α/β_H-spectrin-Duf interaction is also required for stabilizing the mechanoaccumulative α/β_H-spectrin at the fusogenic synapse.

Despite the largely “co-localization” of α/β_H-spectrin and Duf at the fusogenic synapse observed with confocal microscopy, structured illumination microscopy (SIM) revealed distinct microdomains occupied by these proteins at early stages of the fusogenic synapse marked by small actin foci (Fig. 6ai), suggesting that Duf does not directly recruit β_H-spectrin in founder cells. β_H-spectrin appeared to surround the actin focus, consistent with the mechanosensitive accumulation of α/β_H-spectrin to the base areas of invasive protrusions. At late stages of the fusogenic synapse characterized by large actin foci and a ring-like structure formed by β_H-spectrin and Duf, these two proteins exhibited closer

association, likely mediated by α/β_H-spectrin-Duf interaction (Fig. 6aii). Strikingly, α/β_H-spectrin was mostly seen at the outer rim of the ring (Fig. 6aii), indicating that the spectrin network functions as a cellular fence to restrict Duf diffusion.

α/β_H-spectrin network functions as a cellular sieve to constrict the invasive protrusions

The closely abutting morphology of the invasive protrusions in *α/β_H-spectrin* mutant prompted us to ask whether spectrin is involved in shaping the invasive structure to well separated, long and narrow protrusions. At early stages of the fusogenic synapse, actin polymerization in the FCM propelled wide protrusions that triggered mechanosensitive accumulation of β_H-spectrin at the base (Fig. 6bi-ii). Along with foci growth, more β_H-spectrin accumulated to the fusogenic synapse, resulting in an uneven spectrin network with smaller spectrin-free domains (Fig. 6biii). At the late stage, only narrow protrusions were seen penetrated through spectrin-free microdomains (Fig. 6biii-v; Supplementary Video 10). Thus, the spectrin network in the founder cell functions as a "cellular sieve" to constrict the diameters of the invasive protrusions from the FCM. The resulting long and narrow protrusions put the fusogenic synapse under high mechanical tension to promote plasma membrane fusion[12, 14].

βV-spectrin is required for mouse myoblast fusion

The requirement for β_H-spectrin in *Drosophila* myoblast fusion led us to test whether the mammalian ortholog of β_H-spectrin, βV-spectrin (also known as Sptbn5), is involved in myoblast fusion. Knocking down βV-spectrin with two independent siRNAs in mouse C2C12 myoblasts significantly decreased C2C12 cell fusion, respectively (Fig. 7a, b, c). This was not due to a failure in muscle cell differentiation, as the expression level of myogenic regulatory factors, MyoD and Myogenin, remained similar in knockdown vs. control cells (Fig. 7d, e; Supplementary Fig. 5b). In addition, the expression of skeletal muscle structural protein, skMHC, was not affected by the knockdown (Fig. 7e). Consistent with the normal expression of these proteins, the βV-spectrin knockdown cells had a normal, elongated morphology and are MHC positive, despite containing fewer nuclei compared to the control myofibers (Fig. 7a). Thus, like its *Drosophila* counterpart, βV-spectrin promotes mammalian myoblast fusion.

DISCUSSION

This study has revealed a dynamic mechanoresponsive property of α/β_H-spectrin in response to invasive forces during cell-cell fusion. The mechanosensitive accumulation of α/β_H-spectrin in the receiving fusion partner establishes a transient and uneven spectrin-enriched network at the fusogenic synapse, which functions both as a cellular fence to restrict cell adhesion molecules and a cellular sieve to constrict the invasive protrusions from the attacking cell. Through these actions, spectrin helps to build a fusogenic synapse under high mechanical tension to facilitate cell membrane fusion.

An intercellular mechanoresponsive feedback loop at the fusogenic synapse

The fusogenic synapse is established by trans-interactions between cell type-specific CAMs, which initiate a series of downstream cellular events in both cell types[15, 45–47]. In FCMs,

Sns recruits the Arp2/3 NPFs to activate actin polymerization and generate invasive protrusions, which triggers mechanosensitive accumulation of α/β_H-spectrin in the apposing founder cells. The accumulated α/β_H-spectrin keeps Duf at the fusogenic synapse, which recruits additional Duf by lateral diffusion and oligomerization. Newly recruited Duf and transiently stabilized Sns will set off additional rounds of protrusion formation, mechanosensitive accumulation of α/β_H-spectrin, and recruitment of additional CAMs. Through such a positive feedback loop, a mature fusogenic synapse forms with appropriate levels and localization of CAMs, actin and spectrin. The absence of α/β_H-spectrin in founder cells breaks the positive feedback loop, such that Duf and Sns cannot maintain/increase their concentrations at the fusogenic synapse and the structure eventually falls apart. Thus, the intercellular mechanoresponsive feedback loop is critical for the growth and stabilization of the fusogenic synapse.

α/β_H-spectrin as a dynamic mechanoresponsive protein for shear deformation

Spectrin has long been thought as a scaffolding protein that stably links the plasma membrane and the actin cytoskeleton. Our study revealed a mechanosensitive behavior of α/β_H-spectrin in response to shear stress (Supplementary Fig. 6a). Under shear stress, the actin network's shape/angle change leads to changes in the distances between actin crosslinker binding sites. While shorter and stiffer crosslinkers are prone to dissociating from the network, α/β_H-spectrin heterotetramers, each with 29 spectrin repeats and flexible linker regions, can accommodate a range of angle/distance changes by folding or unfolding the spectrin repeats and stay bound to the shear-deformed actin network for an extended period of time, In this regard, it has been demonstrated that spectrin heterotetramers in red blood cells unfold their spectrin repeats under shear stress[48]. FRAP analyses revealed a fraction of α/β_H-spectrin that remains associated with the actin network at the fusogenic synapse, consistent with the prolonged binding of some spectrin heterotetramers. We propose that the extensibility and flexibility of α/β_H-spectrin heterotetramers are the two major properties enabling its transient stable association with the shear-deformed actin network. In support of this, filamin, an actin crosslinker organized as flexible and extensible V-shaped dimers (having Ig-like folds[49] instead of spectrin repeats), also exhibited mechanosensitive accumulation under shear stress[42].

Once the shear stress is removed from the cell cortex, the actin network is no longer under strain and α/β_H-spectrin dissociates from the actin network, generating a pool of free α/β_H-spectrin heterotetramers available for future mechanosensitive responses. Two factors may influence the dynamic dissociation of spectrin from actin: accessory proteins and the actin-binding affinity of spectrin. The absence of adducin and protein 4.1 in embryonic muscle cells suggests that the α/β_H-spectrin-actin interaction is relatively unstable compared to that in erythrocytes and axons, such that α/β_H-spectrin is more likely to dissociate from the actin network in muscle cells. Although the actin-binding affinities of the structurally similar β_H-spectrin and β-spectrin are not known, the difference in their mechanoresponsive behaviors suggests that β-spectrin, similar-sized as mini-β_H-spectrin, may bind F-actin with a higher affinity than β_H-spectrin/mini-β_H-spectrin. Thus, most β-spectrin proteins are stably integrated into the α/β-spectrin heterotetramers at the cell cortex, leaving few free β-spectrin available for transient mechanosensitive response at the fusogenic synapse. In this regard, α-

actinin-1, which has a 90-fold higher actin-binding activity than α-actinin-4, does not show mechanosensitive accumulation as does α-actinin-4[50].

The α/β_H-spectrin network functions as a cellular fence and a cellular sieve

The mechanoaccumulative spectrin network serves at least two functions at the fusogenic synapse. In founder cells, the accumulated spectrin builds a cellular fence to restrict Duf diffusion, likely through two complementary mechanisms (Supplementary Fig. 6b). First, biochemical interactions between Duf and spectrin could prevent Duf clusters from lateral diffusion when they encounter spectrin-enriched patches. Second, the spectrin heterotetramers are linked to plasma membrane via β_H-spectrin's PH domain and may collide with Duf's cytoplasmic domain to block Duf diffusion. A similar role for spectrin in restricting transmembrane protein diffusion has been demonstrated in mouse erythrocytes, in which the transmembrane protein band 3 diffuses faster in spectrin deficient mutant erythrocytes than in normal cells[51] and the cytoplasmic portion of band 3 slows down the diffusion of the protein[52]. Spectrin also functions as a cellular sieve to constrict the invasive protrusions from the FCM (Supplementary Fig. 6b). The buildup of the sieve is a dynamic process involving continuous mechanical stimulation and mechanosensitive accumulation. The early mechanosensitive accumulations of spectrin in founder cells locally block future protrusions from the FCM, forcing new protrusions to penetrate through neighboring spectrin-free areas, thus triggering additional spectrin accumulation. Eventually, large areas of the fusogenic synapse will be populated by spectrin heterotetramers, forming an uneven spectrin network with a few spectrin-free microdomains. Only narrow protrusions that have sufficient mechanical stiffness can "squeeze" through these microdomains to invade the founder cell deeply (Supplementary Fig. 6b). Thus, the dynamically accumulated spectrin network gradually constricts the invasive protrusions from the FCM and increases the mechanical tension at the fusogenic synapse to promote cell-cell fusion. Given the widespread expression of spectrin in most eukaryotic cell types, our characterization of α/β_H-spectrin as a dynamic mechanoresponsive protein in fusogenic cells has broad implications for understanding spectrin functions in many dynamic cellular processes beyond cell-cell fusion.

Methods

Fly stocks and genetics

The following strains were obtained from the Bloomington *Drosophila* Stock Center: Fly stocks w^{1118} (wild type), α-$spec^{rg41}$ (α-*spec* mutant), $kst^{MI03134}$(β_H-*spec* trap line tagged by GFP and 3xFlag; labeling the two longer protein isoforms, PE and PG), *twi-GAL4*, *mef2-GAL4*, *69B-GAL4*, *UAS-GFP-actin*, and *UAS-actin-mRFP*. $kst^{CPTI002266}$ (β_H-*spec* trap line tagged by YFP; labeling the 5 shorter protein isoforms, PA, PB, PC, PF and PH) was obtained from the Kyoto Stock Center. Other stocks used were: $kst^{14.1}$ (β_H-*spec* mutant)[53], *Df(3L)1226* (β_H-*spec* deficiency line)[53], *UAS-mini-*β_H*-Spec*[54], *UAS-Myc-β-Spec*[23], *UAS-DufΔintra-Flag*[33], $dpak3^{zyg(del)19}$, $sltr^{S194643}$, *sns-GAL4*[55], and *rP298-GAL4*[35]. Transgenic flies carrying *UAS-V5-*β_H*-Spec*, *UAS-mCherry-*β_H*-Spec*, *UAS-Duf-GFP* and *UAS-Duf-mCherry* were generated by P-element-mediated germline transformation. To express genes in fly embryos, females carrying the transgene under the control of an *UAS* promoter were

crossed with *twi-GAL4* (all muscle cells), *mef2-GAL4* (all muscle cells), *rP298-GAL4* (founder cells), *sns-GAL4* (FCMs) and *69B-GAL4* (epithelial cells) males, respectively. Expression of β_H-Spec in FCMs was performed in a fusion-defective *sltr* mutant[43] to prevent diffusion of ectopically expressed β_H-Spec from FCMs to founder cells following myoblast fusion events such as in wild-type embryos. α/β_H-spectrin double mutant, α-*spec*^{rg41},*kst*$^{14.1}$/*TM6* (labeled as α-*spec*$^{-/-}$,β_H-*spec*$^{-/-}$ in figures), was generated using standard genetic methods.

Molecular biology

Full-length β_H-*spec* was amplified by PCR (with or without a tag) from cDNAs generated from mRNA of stage 11–15 *w*^{1118} flies. Due to the large size of *the* β_H-*spec* gene, three fragments were individually amplified using the primers as follows:

1. β_H-spec-5': GACCGGTCAACATGACCCAGCGGGACGGCATC
2. β_H-spec-3721–3': CTCCACGAATTCGGTGTCATG
3. β_H-spec-3721–5': CATGACACCGAATTCGTGGAG
4. β_H-spec-8214–3': CTCACCCTCTAGAATGCTATTG
5. β_H-spec-8214–5': CAATAGCATTCTAGAGGGTGAG
6. β_H-spec-3': CCAAGCGGCCGCTCACTGTGGCGGGACTTGACTC

The three PCR fragments were then subcloned into a *Drosophila* transformation vector pUAST. To generate the UAS-β_H-*Spec*ΔN and UAS-β_H-*Spec*ΔC constructs, the following primers were used:

1. β_H-spec-3865–5': GGAATTCCAACATGGTGTGTCGATCTGCAAATGTTC
2. β_H-spec-8028–3': GGTCTAGATCACAGCTGATGGGCCTCAGTTAG

To generate pDEST-β_H-*Spec* constructs for GST-fusion proteins for the F-actin co-sedimentation assays, the Gateway cloning system was used (Invitrogen) with the following primers:

1. β_H-spec-1-C: GGGGACAAGTTTGTACAAAAAAGCAGGCTTCATGACCCAGCGGGACGGCATC
2. β_H-spec-1-K: GGGGACCACTTTGTACAAGAAAGCTGGGTTTTACTTCTTGCGATCTGCGTCCAT
3. β_H-spec-29-C: GGGGACAAGTTTGTACAAAAAAGCAGGCTTCGGAGCCAAACAAGTCCACGTC
4. β_H-spec-31-K: GGGGACCACTTTGTACAAGAAAGCTGGGTTTTATTGGGACGCCGCATTCTGGCG

5. β_H-spec-34-C: GGGGACAAGTTTGTACAAAAAAGCAGGCTTCCCGAACATGCAACTGCTTAGC

6. β_H-spec-34-K: GGGGACCAC TTTGTACAAGAAAGCTGGGTTTTATCACTGTGGCGGGACTTGACT

Full-length *β-spec* was amplified by PCR from the UAST-Myc-*β-spec* plasmid[23]. The original construct lacks nine residues at the N-terminus, which was restored in this subcloning. Due to the large size of *the β-spec* transgene, two fragments were individually amplified using the primers as follows:

1. β-spec-5': TCGAACGCTGCTATACGATCGGGCGGCCGCATGACGACGGACATTTCGATTGTTCGCTGGGATCCCAGCCAGGGTCCTGGCA

2. β-spec-int-3': GTTGTCGATCTCCTCGCGGATCG

3. β-spec-int-5': CGATCCGCGAGGAGATCGACAAC

4. β-spec-3': accttcgaaccgcgggcccTCTAGATTACTTTTTCTTTAAAGTAAAAAACGATCTGCGCT

The two PCR fragments were then subcloned into a *Drosophila* vector pAc-mCherry (N) by Gibson assembly. pAc-mCherry (N) was modified from pAc5.1/V5-His vector (Invitrogen), into which mCherry was PCR-cloned between KpnI and NotI sites, using the primers as follows:

1. mCherry-5': CGTGGTACCATGGTGAGCAAGGGCGAGG-3' (forward)

2. mCherry-linker-GCAGCGGCCGCCCGATCGTATAGCAGCGTTCGACTTGTACAGCTCGTCCATGC. The resulting linker residues between the N-terminal mCherry and β-spec are SNAAIRSGGR.

N-terminally mCherry-tagged full-length α-spectrin was generated by inserting mCherry into pBSK-α-spectrin construct (from C. Thomas) by Gibson assembly. This created de-novo AgeI site upstream of Kozak sequence (GCC ACC) followed by mCherry sequence, flexible linker sequence and the full-length α-spectrin. The AgeI-NotI piece containing mCherry and full-length α-spectrin was subsequently subcloned into the fly expression vector pAc-V5-His (Invitrogen). The primer pair used to create mCherry-Linker tag for Gibson assembly is as follows:

1. mCh-α-spec-For: GAG CTC CAC CGC GGT GGC GGC CGC ACC GGT GCC AAC ATG GTG AGC AAG GGC GAG GAG

2. mCh-α-spec-Rev: CAC CTC TTT GGG TGT AAA GTT CTC CAT CGA TCG TAT AGC AGC ATT CGA CTT GTA CAG CTC GTC CAT GCC

dsRNAs were synthesized by *in vitro* transcription with gene-specific primers containing the T7 promoter sequence (TTAATACGACTCACTATAGGGAGA) at the 5' end (MEGAscript; Ambion). Synthesized dsRNAs were purified using NucAway™ Spin Columns (Ambion).

Immunofluorescent staining and imaging

Fly embryos were fixed and stained as described previously[4, 43]. The following primary antibodies were used: rabbit anti-muscle myosin heavy chain (1:1000)[56], rabbit anti-β_H-spectrin (1:100)[21], rabbit anti-β-spectrin (1:400)[57], mouse anti-α-spectrin (1:1; DSHB; 3A9), guinea pig anti-Duf (1:500)[4], guinea pig anti-Ants (1:1000)[34], rat anti-Sltr (1:30)[43], rat anti-Sns (1:500)[30], mouse anti-Eve (1:30; DSHB; 3C10), mouse anti-adducin (1:400; DSHB; 1B1), mouse anti-protein 4.1 (1:400; DSHB; C566.9), rabbit anti-GFP (1:500; Invitrogen; A-11122), mouse anti-Flag (1:200; Sigma; F3165), mouse anti-Myc (1;100; Thermo Fisher Scientific; MA1–980) and mouse anti-V5 (1:200; Invitrogen; R960–25). The following secondary antibodies were used at 1:200: Alexa488-, Alexa568-, and Alexa647-conjugated (Invitrogen) and biotinylated (Vector Laboratories) antibodies made in goats. For phalloidin staining, FITC- or Alexa568-conjugated phalloidin (Invitrogen) were used at 1:200. Fluorescent images were obtained on an LSM 700 Meta confocal microscope (Zeiss), acquired with LSM Image Browser software (Zeiss) and Zen software (Zeiss), and processed using Adobe Photoshop CS. For quantification of fluorescent signals, the signal intensities of cellular area of interest and control area were measured and processed for presentation by the Image J program (http://imagej.nih.gov/ij/).

Drosophila cell culture

S2 and S2R+ cells were cultured in Schneider's medium (Gibco) supplemented with 10% fetal bovine serum (FBS) (Gibco) and penicillin/streptomycin (Sigma). Cells were transfected using Effectene (Qiagen) per the manufacturer's instructions. For immunofluorescent staining, cells were fixed with 4% formaldehyde in PBS, washed in PBST (PBS with 0.1% Triton X-100) and PBSBT (PBST with 0.2% BSA) consecutively, and stained with the following antibodies in PBSBT: mouse α-V5 (1:2000; Invitrogen; R960–25) and rabbit α-GFP (1:1000; Invitrogen; A-11122). Secondary Alexa488-, Alexa568-, or Alexa647-conjugated antibodies were used at 1:400 (Invitrogen). To visualize F-actin, FITC- or Alexa 568-conjugated phalloidin (Invitrogen) was used at 1:500 in PBST.

Mouse C2C12 myoblast culture

A pair of predesigned siRNAs against the mouse βV-spectrin gene (siRNA1, βV-spectrin-1: CAGGATGGGCTTCGAACCCTA; siRNA2, βV-spectrin-2: AAAGACGATTTCAAGCCCTAA) were obtained from Qiagen. RNAi was performed per manufacturer's instructions. Briefly, approximately 3×10^5 cells were seeded on each well of a 6-well tissue culture dish and transfected with the individual siRNAs against βV-spectrin (10uM final concentration) using HiPerFect transfection reagent (Qiagen). On day 2, the cells were transfected again and differentiated, and cells that were treated in parallel were subjected to qRT-PCR to access the knockdown (KD) level. Five days post-differentiation, cells were fixed and stained with anti-skeletal muscle myosin antibody (1:100; Santa Cruz Biotechnology; F59, sc-32732) to identify differentiated cells. Cells were mounted using Prolong Gold antifade reagent with DAPI (Molecular Probes, Invitrogen) to visualize the

nuclei. The fusion index was calculated as the percentage of nuclei in multinucleated syncytia versus total number of nuclei per 20X microscopic fields under LSM 810 (Zeiss). Cells in at least 10 random fields were counted in each experiment and three independent experiments were performed.

For western blot analyses and quantifications, transfected control and siRNA-treated C2C12 cells were collected at different time points, and washed and lysed in cell lysis buffer (0.5% SDS, 1% NP-40, 1% sodium deoxycholate, 150mM NaCl, 2mM EDTA and 10 mM sodium phosphate, pH 7.2) containing protease inhibitors. The cell lysates were briefly sonicated, centrifuged, analyzed by SDS-PAGE and western blotting with antibodies against MyoD (1:100; sc-377460), Myogenin (1:100; sc-52903), skeletal muscle myosin (1:100; sc-32732) and α-tubulin (1:100; sc-58666) from Santa Cruz Biotechnology. Protein quantification was performed using the photoshop image software (adobe). The chemiluminal emission from both the protein of interest and the loading control were manually tested to be within the linear range. For each experiment, three independent preparations were examined.

Time-lapse imaging and fluorescent recovery after photobleaching (FRAP)

Time-lapse imaging of embryos was performed as previously described[4]. Briefly, embryos expressing fluorescently tagged proteins in muscle or epithelial cells were collected and dechorionated in 50% bleach. Subsequently, embryos were washed in water, placed onto a double-sided tape (3M), and covered with a layer of Halocarbon oil 700/27 (2:1; Sigma). Time lapse image acquisition was carried out on an LSM 700 Meta confocal microscope (Zeiss).

The FRAP experiments were performed using the same conditions described in Jin et al., which allowed full fluorescence recovery of GFP-actin, GFP-WASP and Sltr-mCherry[18]. Specifically, the solid 488 nm laser output was set to 2% to avoid general photobleaching and phototoxicity. A region of interest (ROI) was manually selected and imaged in 3 to 5 frames every 30 sec to record the original fluorescent intensity (pre-bleach). Then the ROI was quickly photobleached to a level ~20% of its original fluorescence intensity by 5–10 times of consecutive 3-sec laser scans with 2% laser output and subsequently imaged every 30 sec to record fluorescence recovery (post-bleach). The fluorescence intensities of the pre- and post-bleached ROI were measured using the image J program. The Prism software was used to determine the maximal recovery level (the percentage recovery compared to the pre-bleach level) and the half-time of recovery using a kinetic curve fit with an exponential decay equation.

Structured illumination microscopy (SIM)

Stage 13–14 embryos were fixed and stained as described above. The samples were then mounted in Prolong Gold (Molecular Probes) and imaged with an inverted microscope (Ti-E; Nikon) equipped with a 100x oil NA1.49 CFI SR Apochromat TIRF objective lens and an ORCA-Flash 4.0 sCMOS camera (Hamamatsu Photonics K.K.). The images were processed using Adobe Photoshop CS6.

Electron microscopy

Embryos were fixed by the high-pressure freezing and freeze substitution (HPF/FS) method as previously described[4, 58]. Briefly, a Bal-Tec device was used to freeze stage 12–14 embryos. Freeze-substitution was performed with 1% osmium tetroxide, 0.1% uranyl acetate in 98% acetone and 2% methanol on dry ice. Fixed embryos were embedded in Epon (Sigma-Aldrich) and cut into thin sections with an ultramicrotome (Ultracut R; Leica). The sections were mounted on copper grids and post-stained with 2% uranyl acetate for 10 min and Sato's lead solution[59] for 1 min to improve image contrast. Images were acquired on a transmission electron microscope (CM120; Philips).

Recombinant protein purification and F-actin co-sedimentation assay

To purify GST-fused β_H-spectrin fragments from BL21-DE3 cells (NEB), protein expression was induced with 0.2 mM IPTG at room temperature for 12–15 hours. Cells were harvested and lysed by sonication in the lysis buffer: PBS (pH 7.4), 1% Triton X-100, 5 mM DTT, 1 mM PMSF, and complete-mini protease inhibitor cocktail (Roche). After centrifugation, the supernatant was collected and incubated with pre-equilibrated glutathione-agarose resin at 4°C for 2–3 hours. After washing in the lysis buffer, β_H-spectrin protein was eluted with the elution buffer: 50 mM Tris (pH 7.5), 150 mM NaCl, 5 mM DTT, 10 mM glutathione (Sigma).

F-actin co-sedimentation assay was performed following the manufacturer's protocol (Cytoskeleton). Briefly, 0.5–1 μM purified protein was incubated with 4 μM F-actin assembled from monomeric actin for 1 hour in F buffer: 5 mM Tris-HCl (pH 8.0), 0.2 mM $CaCl_2$, 50 mM KCl, 2 mM $MgCl_2$, 1 mM ATP. The F-actin/protein mixtures were centrifuged at 140,000 g for 30 min, and supernatants and pellets were separated and analyzed by SDS-PAGE and Coomassie Blue staining.

Co-immunoprecipitation (Co-IP)

Embryos expressing GFP-tagged Duf and Flag-tagged β_H-spectrin (*kst*^{MI03134}*/twi-GAL4; UAS-Duf-GFP/+*) were collected and dechorionated in 50% bleach. Embryos were frozen in liquid nitrogen and then dissociated in cold extraction buffer (50 mM Tris-HCl (pH 8.5), 150 mM NaCl, 0.5% sodium deoxycholate) with 20 strokes in a Dounce homogenizer. After centrifugation at 16,000 g for 20 min, supernatants were removed and incubated with either anti-V5 (control) or anti-Flag (β_H-spectrin) antibodies at 4°C for 2–3 hours. Protein-G-Sepharose beads (Roche) were used to pull down proteins. Precipitated proteins were analyzed by SDS-PAGE and western blotting analysis.

Micropipette aspiration (MPA)

Micropipette aspiration was performed as previously described[60]. Briefly, a pressure difference was generated by adjusting the height of a motor-driven water manometer. A fixed pressure of 0.4 nN/μm^2 was applied instantly to the cell cortex of S2 cells with a polished glass pipette approximately 2–2.5 μm in radius. Images were collected in Schneider's medium supplemented with 10% FBS on an Olympus IX81 microscope with a 40x (1.3 NA) objective and a 1.6x optivar, utilizing MetaMorph software and analyzed using ImageJ. After background correction, the fluorescence intensity at the sites of protein

accumulation was normalized against the opposite cortex of the cell (I_b/I_o or I_t/I_o, where I_b, I_t, and I_o is the intensity in the cortex at the base, tip, or opposite side of the cell being aspirated). An ANOVA with Fisher's least significant difference was applied to determine statistical significance.

Atomic force microscopy (AFM)

S2R+ cells were plated on glass coverslips coated with concanavalin A (Sigma, St Louis, MO) and transfected to express fluorescently tagged MyoII and β_H-Spec using Effectene (Qiagen), per manufacturer's instructions. Lateral indentation experiments were conducted 2 days after transfection with a modified Catalyst AFM integrated with an Axio Observer fluorescence microscope (Zeiss). To determine the effect of a localized mechanical force on MyoII and β_H-Spec localization, the cantilever (MLCT with a pyramidal tip, Bruker) was first brought into full contact, at around 50 nN setpoint force, with the glass surface on a cell-free area within 10 μm from a target cell. Next, the cell was laterally translated into the stationary cantilever using the piezoelectric XY stage and the NanoScope software (Bruker). The cantilever tip indented the edge of the cell by 2–5 μm. Cells were simultaneously imaged with a plan-apochromat 63x/1.4 NA oil immersion objective (Zeiss). Time lapse images were taken at 5 second intervals using the Micro-Manager software (http://micro-manager.org/wiki/Micro-Manager).

Coarse-grained molecular mechanics modeling

In the coarse-grained model, the membrane-cortex composite is represented by a triangulated network where the nodes denote the crosslinking positions and the triangles resemble the meshes in the actin network, which is a network structure composed of proteins such as actin, actin crosslinkers, and MyoII. The system energy of the composite at the coarse-grained molecular level is calculated by

$$E_{system} = E_{bending} + E_{inplane} + E_{surface} + E_{volume} \quad \text{(S1)}$$

where $E_{bending}$ is bending energy from the plasma membrane; $E_{in\text{-}plane}$ is the in-plane elastic energy associated with the deformation of actin crosslinkers and the dilation of each mesh; $E_{surface}$ is the surface energy of the whole cell; E_{volume} is the energy associated with the volume conservation of the cell[42, 61, 62]. Specifically, the bending energy $E_{bending}$ mainly contributed by the plasma membrane is written as

$$E_{bending} = \frac{1}{2}\sum_{i,j} k_{bend}\left(1 - \cos(\theta_i - \theta_i^0)\right), \quad \text{(S2)}$$

where k_{bend} is the bending modulus, $\theta_{i,j}$ is the angle between the surface normal to the elements i and j, and θ_i^0 is the reference value of θ_i, at equilibrium. The in-plane free energy $E_{in\text{-}plane}$ has the form of

$$E_{in-plane} = \sum_i V_{WLC}(l_i) + \frac{1}{2}\sum_i k_{dilation}\left(A_i - A_i^0\right)^2. \quad \text{(S3)}$$

The first term $V_{WLC}(l_i)$ is the worm-like-chain energy due to the intermolecular and intramolecular deformations of actin cytoskeletal proteins associated with edge, (l_i). The force in the worm-like-chain model is

$$f_{WLC}(l) = -\frac{\partial V_{WLC}(l)}{\partial x} = -\frac{nk_BT}{p}\left(\frac{1}{4(1-x)^2} - \frac{1}{4} + x\right), x = \frac{l}{l_{\max}} \in (0,1), \quad \text{(S4)}$$

where k_B is the Boltzmann constant, T is the temperature, $2n$ is the number of functional actin crosslinkers between two connected nodes, $l_{\max}$ is the maximum length of edge l, and p is the average persistence length of the actin crosslinkers. The second term in Eq. S3 is the energy due to the dilation/shrinking of individual mesh of area A_i with initial value A_i^0 and a dilation modulus, $k_{dilation}$. $E_{surface}$ is the energy associated with the conservation of global surface area and is written as

$$E_{surface} = \frac{1}{2}k_{surface}\left(A_{total} - A_{total}^0\right)^2, \quad \text{(S5)}$$

where $k_{surface}$ is the global area modulus, A_{total} is the total area of membrane-cortex composite and A_{total}^0 is the initial total area. Similarly, E_{volume} is the energy associated with the conservation of global volume and has the form of

$$E_{volume} = \frac{1}{2}k_{volume}\left(V_{total} - V_{total}^0\right)^2. \quad \text{(S6)}$$

k_{volume} is the global volume modulus. V_{total} and V_{total}^0 are the total volume of the cell and its corresponding equilibrium value, respectively. A surface mesh with 10,000 nodes and 19,996 triangles was created for a spherical cell of radius 5 μm. As a result, the average length of the edges is 70 nm long. For Eq. S4, the average persistence length of actin crosslinkers is on the order of 40 nm, and the average number of actin crosslinkers, n, is 1. The values of the remaining parameters are: k_{bend}=100 k_BT, $\theta_i^0 = 0$, $k_{dilation}$= 100 k_BT, $k_{surface}$= 1000 k_BT, k_{volume}=1000 k_BT. The motion of the nodes is calculated by Brownian dynamics equation where the driving force is the derivative of the system energy with respect to the local position.

The initial configuration of the system was thermally annealed at room temperature until the fluctuation of the system energy was negligible. This configuration was then mapped to the shape of a receiving cell. For simplicity, the protrusion has a cylindrical shape with the

radius r_0 and length l on the surface of a cell with a diameter of 10 μm. The tip of the protrusion was a spherical cap of a radius of r_0. The final state of the system was achieved after 20 sec of Brownian dynamics simulation with a time-step of 10^{-5} sec. The area dilation of each node was determined by averaging of the dilation of the triangles with which the node of interest was associated. The shear deformation of each node was calculated in a similar way. The contour of the deformation on the protrusion was plotted by the software Tecplot (Supplementary Fig. 7). The deformations along the length direction of the protrusion were obtained by the extraction tool of the software.

Code availability

The C programs for the computation of the energy of the cells with protrusions are available from the following website – https://pan.baidu.com/s/1wjroHIyh7eXZQ3IjHGfRUA.

Statistics and Reproducibility

Statistical significance was assessed using two-tailed Student's *t*-test and ANOVA with Fisher's least significant difference. *p* values were obtained using the Microsoft Excel 2010, GraphPad Prism 5, and Kaleidagraph 4.1 softwares. The number of biological replicates for each experiment is indicated in the figure legends. Immunofluorescence images were representatives of at least ten independent samples, MPA images of at least eight independent cells, and western blots of three independent experiments.

Data availability

The main data supporting the findings of this study are available within the article and its Supplementary Information files. All other data supporting the findings of this study are available from the corresponding author upon reasonable request.

Supplementary Material

Refer to Web version on PubMed Central for supplementary material.

Acknowledgements

We thank the Bloomington stock center for fly stocks, Bruce Paterson for the MHC antibody, Fan Li for technical assistance, Guofeng Zhang for help with HPF/FS, Jeremy Nathans for sharing confocal microscopes, and Duojia Pan for critically reading the manuscript. This work was supported by NIH grants (R01 AR053173 and R01 GM098816), American Heart Association Established Investigator Award and HHMI Faculty Scholar Award to E.H.C.; NIH grants (R01 GM66817 and R01 GM109863) to D.N.R; NIH grants (R01 GM074751 and R01 GM114671) to D.A.F; NSF grant #MCB-1122013 to C.T.; NSFC grant #11572316 to T.L., and NSFC grant #31771256 to R.D. R.D. was supported by an AHA postdoctoral fellowship; K.S. by an AHA Scientist Development Grant; D.M.L. by a Canadian Institute of Health Research postdoctoral fellowship; and S.S. by a Life Sciences Research Foundation postdoctoral fellowship.

References

1. Bennett V & Lorenzo DN Spectrin- and ankyrin-based membrane domains and the evolution of vertebrates. Curr Top Membr 72, 1–37 (2013). [PubMed: 24210426]
2. Bennett V & Lorenzo DN An Adaptable Spectrin/Ankyrin-Based Mechanism for Long-Range Organization of Plasma Membranes in Vertebrate Tissues. Curr Top Membr 77, 143–184 (2016). [PubMed: 26781832]

3. Machnicka B et al. Spectrins: a structural platform for stabilization and activation of membrane channels, receptors and transporters. Biochim Biophys Acta 1838, 620–634 (2014). [PubMed: 23673272]
4. Liu SC, Derick LH & Palek J Visualization of the hexagonal lattice in the erythrocyte membrane skeleton. J Cell Biol 104, 527–536 (1987). [PubMed: 2434513]
5. Pielage J et al. A presynaptic giant ankyrin stabilizes the NMJ through regulation of presynaptic microtubules and transsynaptic cell adhesion. Neuron 58, 195–209 (2008). [PubMed: 18439405]
6. Byers TJ & Branton D Visualization of the protein associations in the erythrocyte membrane skeleton. Proc Natl Acad Sci U S A 82, 6153–6157 (1985). [PubMed: 3862123]
7. Xu K, Zhong G & Zhuang X Actin, spectrin, and associated proteins form a periodic cytoskeletal structure in axons. Science 339, 452–456 (2013). [PubMed: 23239625]
8. Hammarlund M, Jorgensen EM & Bastiani MJ Axons break in animals lacking beta-spectrin. J Cell Biol 176, 269–275 (2007). [PubMed: 17261846]
9. Krieg M, Dunn AR & Goodman MB Mechanical control of the sense of touch by beta-spectrin. Nat Cell Biol 16, 224–233 (2014). [PubMed: 24561618]
10. Chen EH & Olson EN Unveiling the mechanisms of cell-cell fusion. Science 308, 369–373 (2005). [PubMed: 15831748]
11. Aguilar PS et al. Genetic basis of cell-cell fusion mechanisms. Trends Genet 29, 427–437 (2013). [PubMed: 23453622]
12. Sens KL et al. An invasive podosome-like structure promotes fusion pore formation during myoblast fusion. J Cell Biol 191, 1013–1027 (2010). [PubMed: 21098115]
13. Shilagardi K et al. Actin-propelled invasive membrane protrusions promote fusogenic protein engagement during cell-cell fusion. Science 340, 359–363 (2013). [PubMed: 23470732]
14. Kim JH et al. Mechanical tension drives cell membrane fusion. Dev Cell 32, 561–573 (2015). [PubMed: 25684354]
15. Kim JH, Jin P, Duan R & Chen EH Mechanisms of myoblast fusion during muscle development. Curr Opin Genet Dev 32, 162–170 (2015). [PubMed: 25989064]
16. Shin NY et al. Dynamin and endocytosis are required for the fusion of osteoclasts and myoblasts. J Cell Biol 207, 73–89 (2014). [PubMed: 25287300]
17. Haralalka S et al. Asymmetric Mbc, active Rac1 and F-actin foci in the fusion-competent myoblasts during myoblast fusion in Drosophila. Development 138, 1551–1562 (2011). [PubMed: 21389053]
18. Jin P et al. Competition between Blown Fuse and WASP for WIP Binding Regulates the Dynamics of WASP-Dependent Actin Polymerization In Vivo. Dev Cell 20, 623–638 (2011). [PubMed: 21571220]
19. Duan R et al. Group I PAKs function downstream of Rac to promote podosome invasion during myoblast fusion in vivo. J Cell Biol 199, 169–185 (2012). [PubMed: 23007650]
20. Dubreuil RR, Byers TJ, Stewart CT & Kiehart DP A beta-spectrin isoform from Drosophila (beta H) is similar in size to vertebrate dystrophin. J Cell Biol 111, 1849–1858 (1990). [PubMed: 2229176]
21. Thomas GH & Kiehart DP Beta heavy-spectrin has a restricted tissue and subcellular distribution during Drosophila embryogenesis. Development 120, 2039–2050 (1994). [PubMed: 7925008]
22. Tjota M et al. Annexin B9 binds to beta(H)-spectrin and is required for multivesicular body function in Drosophila. J Cell Sci 124, 2914–2926 (2011). [PubMed: 21878499]
23. Mazock GH, Das A, Base C & Dubreuil RR Transgene rescue identifies an essential function for Drosophila beta spectrin in the nervous system and a selective requirement for ankyrin-2-binding activity. Mol Biol Cell 21, 2860–2868 (2010). [PubMed: 20573981]
24. Ruiz-Gomez M, Coutts N, Price A, Taylor MV & Bate M Drosophila dumbfounded: a myoblast attractant essential for fusion. Cell 102, 189–198. (2000). [PubMed: 10943839]
25. Gardner K & Bennett V Modulation of spectrin-actin assembly by erythrocyte adducin. Nature 328, 359–362 (1987). [PubMed: 3600811]

26. Ungewickell E, Bennett PM, Calvert R, Ohanian V & Gratzer WB In vitro formation of a complex between cytoskeletal proteins of the human erythrocyte. Nature 280, 811–814 (1979). [PubMed: 471052]
27. Bennett V & Baines AJ Spectrin and ankyrin-based pathways: metazoan inventions for integrating cells into tissues. Physiol Rev 81, 1353–1392 (2001). [PubMed: 11427698]
28. Richardson BE, Beckett K, Nowak SJ & Baylies MK SCAR/WAVE and Arp2/3 are crucial for cytoskeletal remodeling at the site of myoblast fusion. Development 134, 4357–4367 (2007). [PubMed: 18003739]
29. Strunkelnberg M et al. rst and its paralogue kirre act redundantly during embryonic muscle development in Drosophila. Development 128, 4229–39 (2001). [PubMed: 11684659]
30. Bour BA, Chakravarti M, West JM & Abmayr SM Drosophila SNS, a member of the immunoglobulin superfamily that is essential for myoblast fusion. Genes Dev 14, 1498–1511. (2000). [PubMed: 10859168]
31. Galletta BJ, Chakravarti M, Banerjee R & Abmayr SM SNS: Adhesive properties, localization requirements and ectodomain dependence in S2 cells and embryonic myoblasts. Mech Dev 121, 1455–1468 (2004). [PubMed: 15511638]
32. Shelton C, Kocherlakota KS, Zhuang S & Abmayr SM The immunoglobulin superfamily member Hbs functions redundantly with Sns in interactions between founder and fusion-competent myoblasts. Development 136, 1159–1168 (2009). [PubMed: 19270174]
33. Bulchand S, Menon SD, George SE & Chia W The intracellular domain of Dumbfounded affects myoblast fusion efficiency and interacts with Rolling pebbles and Loner. PLoS One 5, e9374 (2010). [PubMed: 20186342]
34. Chen EH & Olson EN Antisocial, an intracellular adaptor protein, is required for myoblast fusion in Drosophila. Dev Cell 1, 705–715 (2001). [PubMed: 11709190]
35. Menon SD & Chia W Drosophila rolling pebbles: a multidomain protein required for myoblast fusion that recruits D-Titin in response to the myoblast attractant Dumbfounded. Dev Cell 1, 691–703 (2001). [PubMed: 11709189]
36. Rau A et al. rolling pebbles (rols) is required in Drosophila muscle precursors for recruitment of myoblasts for fusion. Development 128, 5061–73. (2001). [PubMed: 11748142]
37. Menon SD, Osman Z, Chenchill K & Chia W A positive feedback loop between Dumbfounded and Rolling pebbles leads to myotube enlargement in Drosophila. J Cell Biol 169, 909–920 (2005). [PubMed: 15955848]
38. Mohler WA et al. The type I membrane protein EFF-1 is essential for developmental cell fusion. Dev Cell 2, 355–362 (2002). [PubMed: 11879640]
39. Stauffer TP, Ahn S & Meyer T Receptor-induced transient reduction in plasma membrane PtdIns(4,5)P2 concentration monitored in living cells. Curr Biol 8, 343–346 (1998). [PubMed: 9512420]
40. Bennett V & Healy J Membrane domains based on ankyrin and spectrin associated with cell-cell interactions. Cold Spring Harb Perspect Biol 1, a003012 (2009). [PubMed: 20457566]
41. Graveley BR et al. The developmental transcriptome of Drosophila melanogaster. Nature 471, 473–479 (2011). [PubMed: 21179090]
42. Luo T, Mohan K, Iglesias PA & Robinson DN Molecular mechanisms of cellular mechanosensing. Nat Mater 12, 1064–1071 (2013). [PubMed: 24141449]
43. Kim S et al. A critical function for the actin cytoskeleton in targeted exocytosis of prefusion vesicles during myoblast fusion. Dev Cell 12, 571–586 (2007). [PubMed: 17419995]
44. Massarwa R, Carmon S, Shilo BZ & Schejter ED WIP/WASp-based actin-polymerization machinery is essential for myoblast fusion in Drosophila. Dev Cell 12, 557–569 (2007). [PubMed: 17419994]
44. Abmayr SM & Pavlath GK Myoblast fusion: lessons from flies and mice. Development 139, 641–656 (2012). [PubMed: 22274696]
45. Krieger CC et al. Cysteine shotgun-mass spectrometry (CS-MS) reveals dynamic sequence of protein structure changes within mutant and stressed cells. Proc Natl Acad Sci U S A 108, 8269–8274 (2011). [PubMed: 21527722]

46. Schejter ED Myoblast fusion: Experimental systems and cellular mechanisms. Semin Cell Dev Biol 60, 112–120 (2016). [PubMed: 27423913]
47. Deng S, Azevedo M & Baylies M Acting on identity: Myoblast fusion and the formation of the syncytial muscle fiber. Semin Cell Dev Biol 72, 45–55 (2017). [PubMed: 29101004]
48. Krieger CC et al. Cysteine shotgun-mass spectrometry (CS-MS) reveals dynamic sequence of protein structure changes within mutant and stressed cells. Proc Natl Acad Sci U S A 108, 8269–8274 (2011). [PubMed: 21527722]
49. Popowicz GM, Schleicher M, Noegel AA & Holak TA Filamins: promiscuous organizers of the cytoskeleton. Trends Biochem Sci 31, 411–419 (2006). [PubMed: 16781869]
50. Schiffhauer ES et al. Mechanoaccumulative Elements of the Mammalian Actin Cytoskeleton. Curr Biol 26, 1473–1479 (2016). [PubMed: 27185555]
51. Sheetz MP, Schindler M & Koppel DE Lateral mobility of integral membrane proteins is increased in spherocytic erythrocytes. Nature 285, 510–511 (1980). [PubMed: 7402296]
52. Tsuji A & Ohnishi S Restriction of the lateral motion of band 3 in the erythrocyte membrane by the cytoskeletal network: dependence on spectrin association state. Biochemistry 25, 6133–6139 (1986). [PubMed: 3790510]
53. Thomas GH et al. Drosophila betaHeavy-spectrin is essential for development and contributes to specific cell fates in the eye. Development 125, 2125–2134 (1998). [PubMed: 9570776]
54. Lee SK & Thomas GH Rac1 modulation of the apical domain is negatively regulated by beta (Heavy)-spectrin. Mech Dev 128, 116–128 (2011). [PubMed: 21111816]
55. Kocherlakota KS, Wu JM, McDermott J & Abmayr SM Analysis of the cell adhesion molecule sticks-and-stones reveals multiple redundant functional domains, protein-interaction motifs and phosphorylated tyrosines that direct myoblast fusion in Drosophila melanogaster. Genetics 178, 1371–1383 (2008). [PubMed: 18245830]
56. Wei Q, Rong Y & Paterson BM Stereotypic founder cell patterning and embryonic muscle formation in Drosophila require nautilus (MyoD) gene function. Proc Natl Acad Sci U S A 104, 5461–5466 (2007). [PubMed: 17376873]
57. Byers TJ, Brandin E, Lue RA, Winograd E & Branton D The complete sequence of Drosophila beta-spectrin reveals supra-motifs comprising eight 106-residue segments. Proc Natl Acad Sci U S A 89, 6187–6191 (1992). [PubMed: 1631106]
58. Zhang S & Chen EH Ultrastructural Analysis of Myoblast Fusion in Drosophila, in Cell Fusion: Overviews and Methods. (ed. Chen EH) 275–297 (Humana Press, NJ; 2008).
59. Sato T A modified method for lead staining of thin sections. J Electron Microsc (Tokyo) 17, 158–159 (1968). [PubMed: 4177281]
60. Kee YS & Robinson DN Micropipette aspiration for studying cellular mechanosensory responses and mechanics. Methods Mol Biol 983, 367–382 (2013). [PubMed: 23494318]
61. Discher DE, Boal DH & Boey SK Simulations of the erythrocyte cytoskeleton at large deformation. II. Micropipette aspiration. Biophys J 75, 1584–1597 (1998). [PubMed: 9726959]
62. Li J, Dao M, Lim CT & Suresh S Spectrin-level modeling of the cytoskeleton and optical tweezers stretching of the erythrocyte. Biophys J 88, 3707–3719 (2005). [PubMed: 15749778]

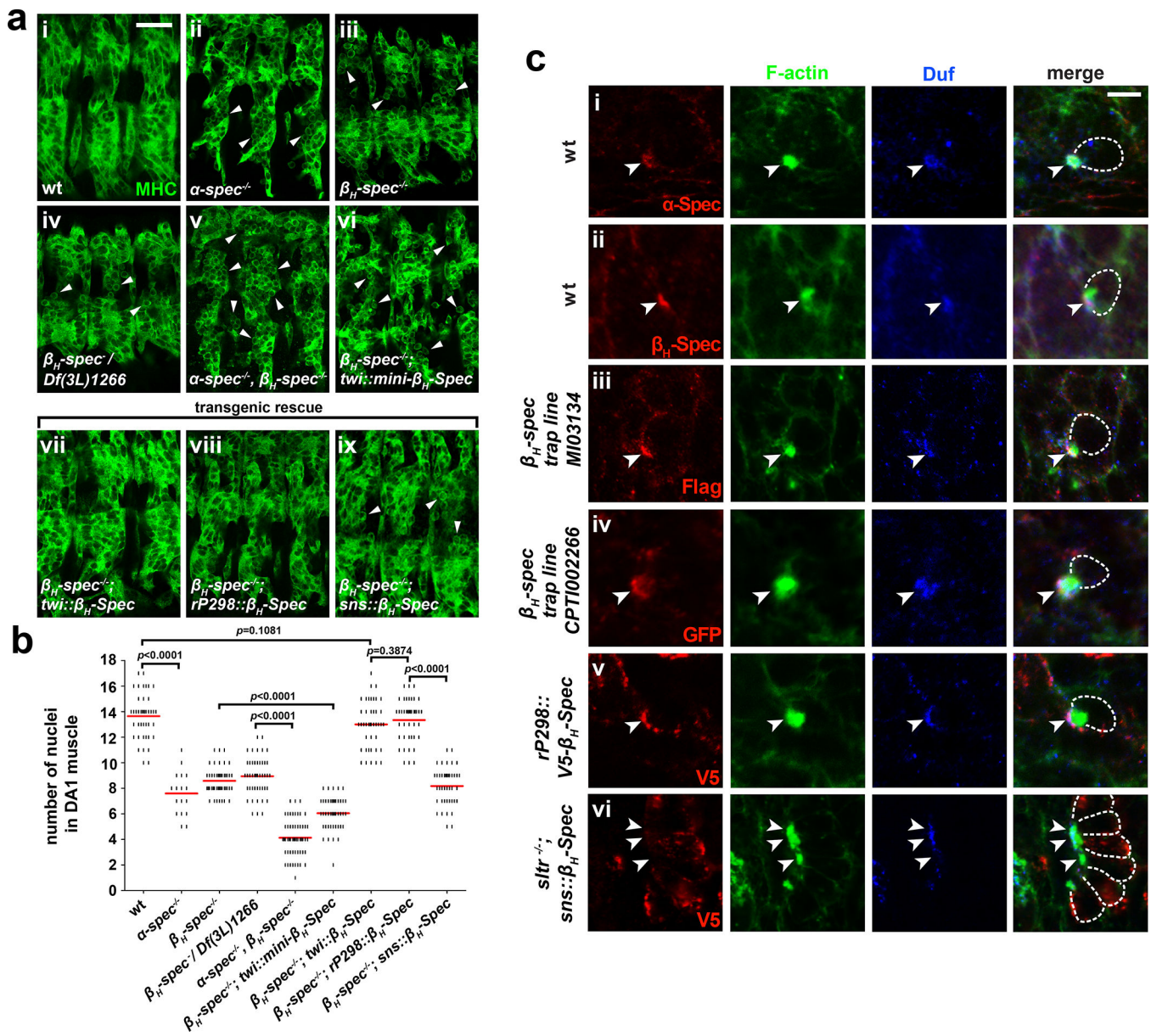

Figure 1. α/βH-spectrin is required for myoblast fusion and enriched at the fusogenic synapse in founder cells

(a) Myoblast fusion phenotype in *α/β$_H$-spectrin* mutant. Stage 15 embryos immunolabeled with anti-muscle myosin heavy chain (MHC). Ventral lateral muscles of three hemisegments shown in each panel. Unfused myoblasts indicted by arrowheads. (i) Wild-type (wt). (ii-iv) Minor fusion defect in *α-spectrin* (*α-spec^{rg41}; α-spec$^{-/-}$*) (ii), *β$_H$-spectrin* (*kst$^{14.1}$; β$_H$-spec$^{-/-}$*) (iii), and transheterozygous *β$_H$-spec^{-}/Df(3L)1266* (iv) mutant. (v) Severe fusion defect in *α/β$_H$-spectrin$^{-/-}$* (*α-spec$^{-/-}$,β$_H$-spec$^{-/-}$*) double mutant. (vi) Expressing mini-βH-spectrin (mini-βH-Spec) in all muscle cells with *twi-GAL4* exacerbated the fusion defect in *β$_H$-spec$^{-/-}$* mutant. (vii-ix) The fusion defect in *β$_H$-spec$^{-/-}$* mutant was rescued by expressing *β$_H$-Spec* in all muscle cells with *twi-GAL4* (vii), in founder cells with *rP298-GAL4* (viii), but not in FCMs with *sns-GAL4* (ix). For each genotype, 10 embryos (biologically independent

samples) were imaged with similar results. Scale bar, 20 μm. (b) Quantification of the fusion index. The number of Eve-positive nuclei in the dorsal acute muscle 1 (DA1) was counted for each genotype in (a). The number (n) of DA1 analyzed for each genotype: n = 42, 17, 45, 45, 55, 45, 42, 42, and 42 (left to right). Horizontal bar, mean value. Statistical significance was determined by the two-tailed Student's t-test (*p* values marked at the top). (c) Localization of α/β_H-spectrin at the fusogenic synapse. Confocal images of side-by-side pairs of FCM (outlined) and founder cell in stage 13–14 embryos triple labeled with phalloidin (F-actin; green), anti-Duf (blue), and anti-α-Spec(i), anti-β_H-Sec(ii), anti-Flag (GFP/Flag trap line; iii), anti-GFP (YFP trap line; iv), or anti-V5 [V5-β_H-Spec expressed in founder cells with *rP298-GAL4* (v) or FCMs with *sns-GAL4* (vi)] in red. Expression of β_H-Spec in FCMs was visualized in the fusion-defective *sltr* mutant without β_H-Spec diffusion from FCMs to founder cells. Note the enrichment of α-Spec (i) and β_H-Spec (ii-iv) at the fusogenic synapse (arrowhead), and specifically in founder cells (v), but not in FCMs (vi). For each genotype, 20 fusogenic synapses (biological independent samples) were imaged with similar results. Scale bar, 5 μm.

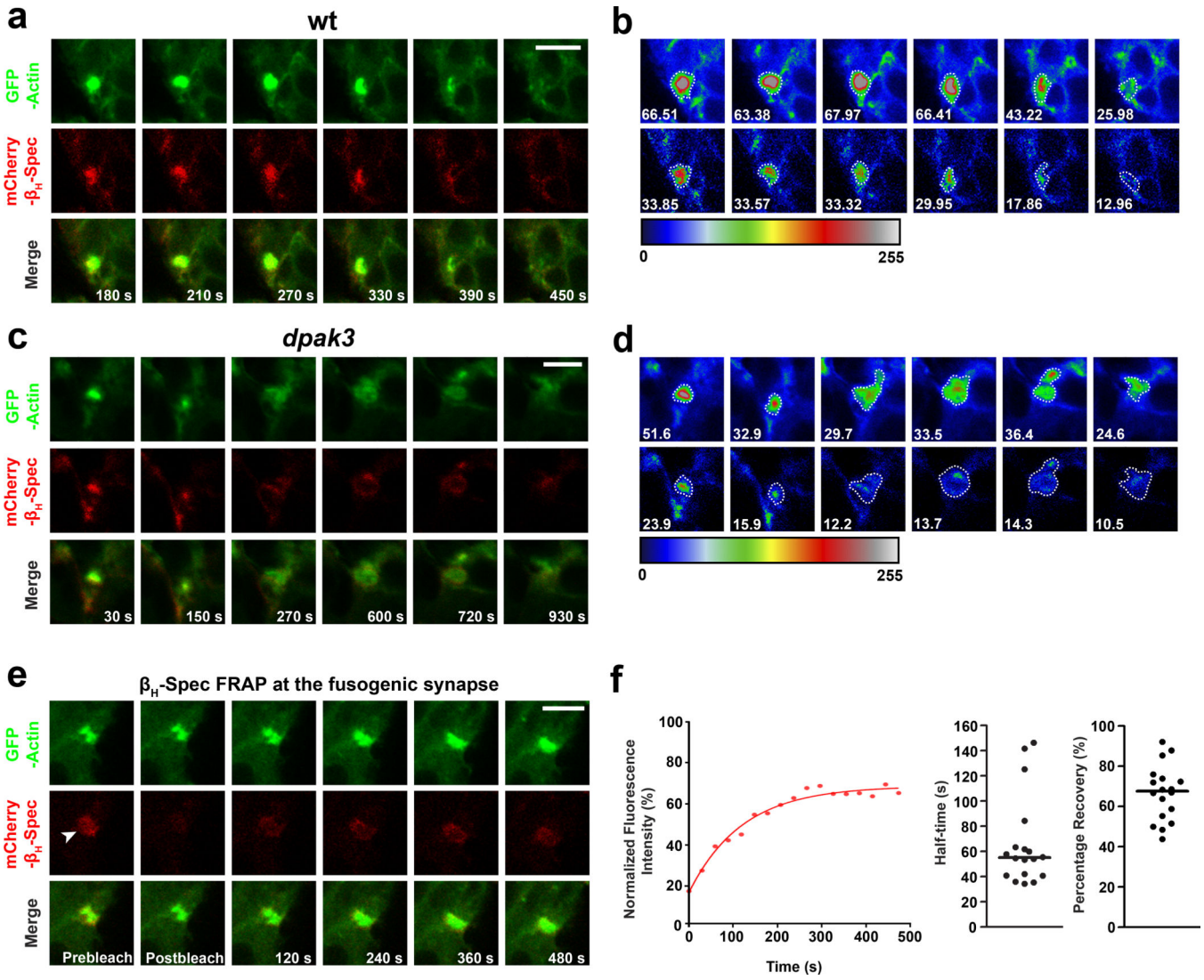

Figure 2. α/β_H-spectrin dynamically accumulates at the fusogenic synapse in response to PLS invasion

(a-d) Time-lapse stills of stage 14 wt (a, b) or *dpak3* mutant (c, d) embryos expressing GFP-actin (green) and mCherry-β_H-Spec (red). The fluorescence intensity of F-actin foci and β_H-Spec accumulation was displayed by heat maps (b and d) on a scale from 0 to 255. The dashed outlines delineate F-actin foci and β_H-Spec accumulation at the fusogenic synapse. The mean fluorescence intensity in the outlined area is shown in each panel. Note the dynamic changes in the intensity and morphology of β_H-Spec accumulation correlating with those of the F-actin foci. For each genotype, 10 fusogenic synapses were live imaged with similar results. Scale bars, 5 μm. (e-f) FRAP of β_H-Spec at the fusogenic synapse. (e) Time-lapse stills of a representative FRAP experiment in a stage 14 wt embryo expressing GFP-actin and mCherry-β_H-Spec. Arrowhead indicates the photo-bleached region. Scale bar, 5 μm. (f) Recovery kinetics of the mCherry fluorescence after photobleaching. The curve on the left shows the fluorescence recovery of mCherry-β_H-Spec in (e). The recovery half-time ($T_{1/2}$) and percentage were quantified from multiple experiments. Each data point represents

a fusogenic synapse; n=18 fusogenic synapses were analyzed by FRAP. Horizontal bar, median value. Average $T_{1/2}$ was 66 ± 35 sec (median: 55 sec) and average percentage recovery was 67 ± 14% (median: 68%).

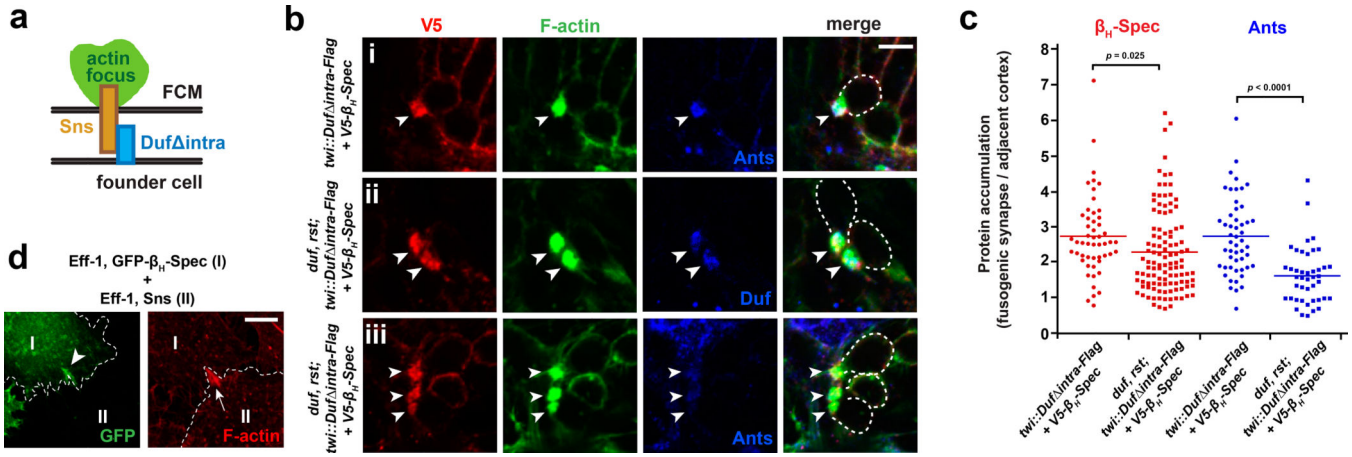

Figure 3. α/β_H-spectrin accumulates at the fusogenic synapse in the absence of chemical signaling from cell adhesion molecules

(a) Schematic diagram of the fusogenic synapse showing truncated Duf (DufΔintra) in the founder cell interacting with Sns in the FCM to induce the formation of an invasive F-actin focus.

(b) Co-expression of DufΔintra-Flag and V5-β_H-Spec in all muscle cells with *twi-GAL4* in wt (i) or *duf,rst* double mutant (ii and iii) embryos. Representative images of fusogenic synapses in stage 13–14 embryos triple labeled with anti-V5 (β_H-Spec, red), phalloidin (F-actin, green), and anti-Ants or anti-Duf (DufΔintra-Flag) in blue. FCMs outlined in the merge panels. Note the β_H-Spec accumulation (ii, iii) and the lack of Ants accumulation (iii) at the fusogenic synapse (arrowheads) in the absence of Duf intracellular signaling. Scale bar, 5 μm. (c) Quantification of the relative intensity of β_H-Spec and Ants enrichment at the fusogenic synapse in wt and *duf,rst* double mutant embryos expressing DufΔintra. The fluorescence intensity at the fusogenic synapse was compared with that in the adjacent cortical area to calculate the relative protein intensity ratio. Each data point represents a fusogenic synapse; n = 52, 111, 51, 43 (left to right) fusogenic synapses were analyzed. Horizontal bar, mean value. Statistical significance was determined by the two-tailed Student's *t*-test (*p* values marked at the top). (d) β_H-Spec enrichment at the fusogenic synapse in S2R+ cells. GFP-β_H-Spec in the receiving cell (I; outlined in the left panel; co-expressing GFP-β_H-spectrin and Eff-1) accumulated at the fusogenic synapse (arrowhead) in response to the F-actin-propelled invasive protrusions (arrow) from the attacking cell (II; outlined in the right panel; co-expressing Sns and Eff-1). 35 fusogenic synapses examined with similar results. Scale bar, 5 μm.

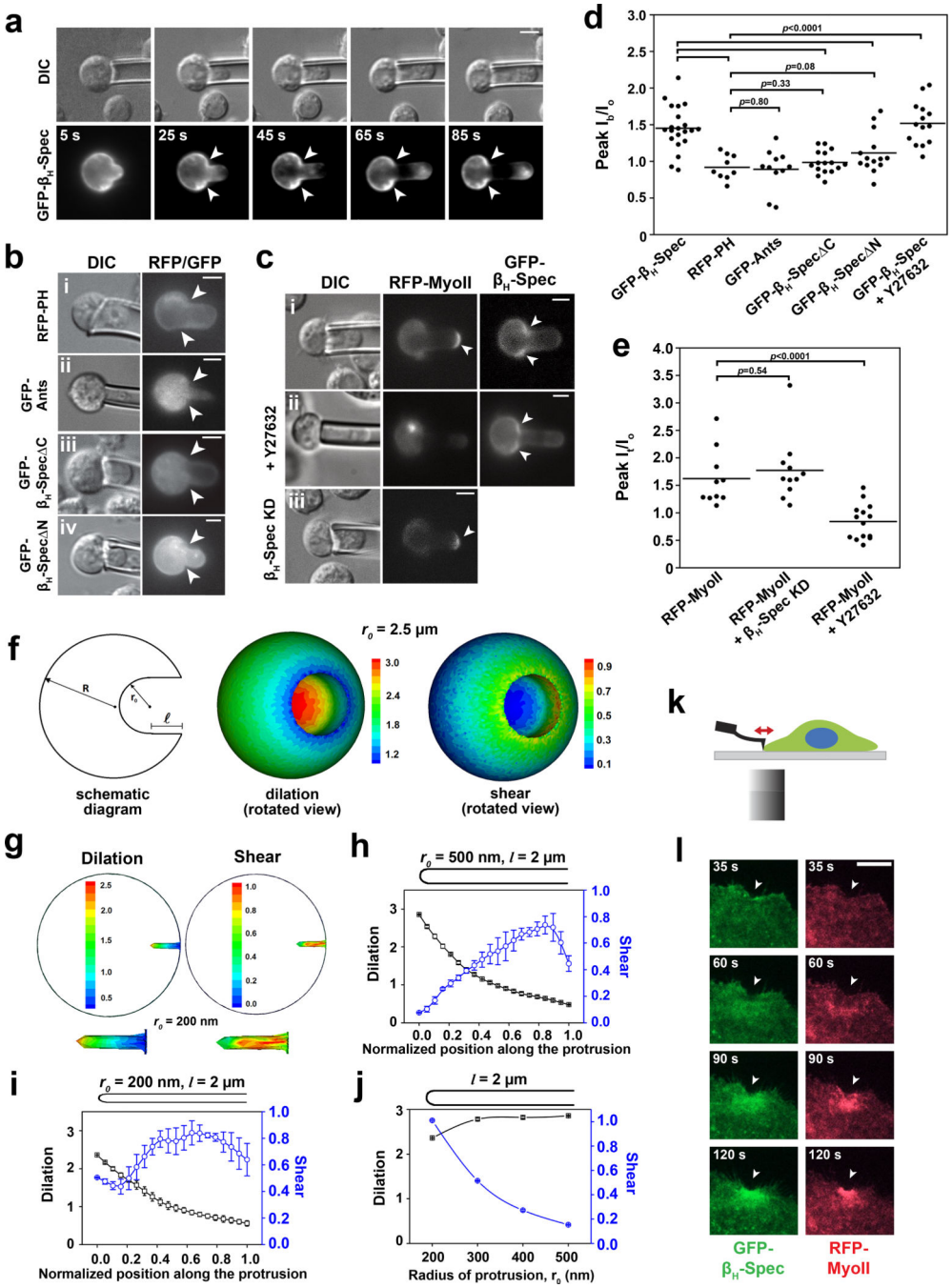

Figure 4. α/β$_H$-spectrin exhibits mechanosensitive accumulation to shear deformation

(a-e) Mechanosensitive accumulation of β$_H$-Spec revealed by MPA. (a-c) Representative images of MPA experiments in which an S2 cell expressing a fluorescent protein was aspirated with a micropipette (diameter ~5 μm). Arrowheads indicate enrichment of GFP-β$_H$-Spec at the base of the aspirated portion in (a), (c*i*) and Y27632-treated cell in (c*ii*); enrichment of RFP-MyoII at the tip in (c*i*) and β$_H$-Spec knockdown (KD) cell (c*iii*); but no enrichment of the probes/proteins in (b). Scale bars, 5 μm. (d-e) Protein accumulation at the base (d) or tip (e) of aspirated cells in (a-c). Background-subtracted fluorescence intensities

at the base (I_b) (d) or tip (I_t) (e) and at the opposite pole of the cell body (I_o) were measured, and the ratio (I_b/I_o) (d) or (I_t/I_o) (e) was calculated. Number of independent experiments: n = 21, 9, 11, 16, 15, 14 (d, left to right) and 10, 11,14 (e, left to right). Horizontal line, mean value. ANOVA with Fisher's least significant difference (*p* values marked at the top). (f-j) Coarse-grained simulation of mechanical deformation in the receiving cell triggered by invasive protrusions. (f-i) Schematic diagram of a cell invaded by a protrusion (f, left panel) and heat maps of simulated dilation or shear deformation (middle/right panels in f; g) caused by protrusions of different radii (r_0). Close-up views in (g). (h and i) Plots of dilation and shear deformation along 2 μm protrusions with an r_0 of 500 nm (h) or 200 nm (i). n=4 independent measurements of deformation along the protrusions, mean +/− SEM. Shear deformation increases at the tip in (i) than (h). (j) Dilation and shear deformations at the tip (normalized position 0.0–0.2) of protrusions with different r_0. Shear deformation increases with smaller radius. (k and l) β_H-Spec accumulation in response to pushing forces revealed by AFM. (k) Schematic diagram of the AFM experiments. A cantilever applied a pushing force to the periphery of S2R+ cell. (l) S2R+ cell expressing GFP-β_H-Spec and RFP-MyoII. Both proteins rapidly accumulated to the indented area generated by the cantilever (arrowheads) in 24 out of 42 cells tested. Scale bar, 10 μm.

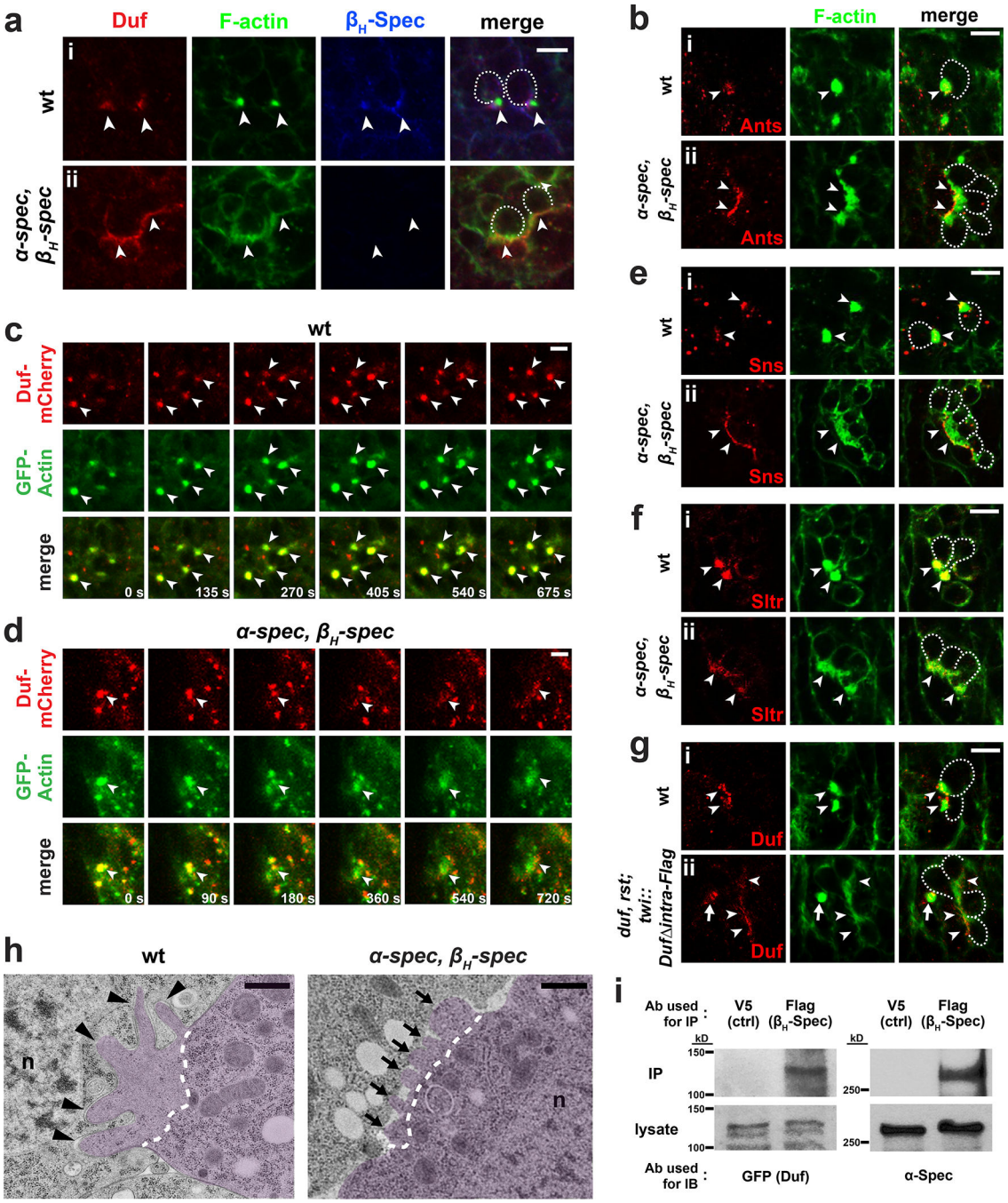

Figure 5. α/β$_H$-spectrin restricts cell adhesion molecules at the fusogenic synapse

(a, b) Duf and Ants in founder cells are dispersed at the fusogenic synapse in *α/β$_H$-spectrin* double mutant. Stage 14 embryos immunolabeled with anti-Duf or anti-Ants (red), phalloidin (green) and anti-β$_H$-Spec (blue). Duf (and Ants) was concentrated in a tight cluster associated with each F-actin focus (arrowheads) in wt (i), but dispersed along with F-actin (arrowheads) in *α/β$_H$-spectrin* mutant (ii). FCMs outlined in merge panels (a, b, e, f and g). (c, d) Time-lapse stills of wt (c) or *α/β$_H$-spectrin* mutant (d) expressing Duf-mCherry (red) and GFP-actin (green). Duf remained in tight clusters associated with F-actin

foci in wt (c), but diffused over time with F-actin in *α/β$_H$-spectrin* mutant (d). (e, f) Sns and Sltr in FCMs are dispersed in *α/β$_H$-spectrin* mutant. Stage 14 embryos immunolabeled with anti-Sns/anti-Sltr (red) and phalloidin (green). (g) Localization of DufΔintra expressed in *duf,rst* mutant embryos. Stage 14 *duf,rst* mutant embryos expressing DufΔintra-Flag with *twi-GAL4* immunolabeled with anti-Duf (red) and phalloidin (green). Note the presence of both dispersed (arrowheads) and clustered (arrow) DufΔintra. In (a) to (g), for each antibody (or fluorophore) combination, 20 (or 10) fusogenic synapses were imaged with similar results. Scale bars, 5 μm. (h) Electron micrographs of the invasive PLS in wt (left) and *α/β$_H$-spectrin* mutant (right). FCMs pseudo-colored in purple. Dash lines delineate the F-actin-enriched area of the PLS. Note the long, narrow and well separated fingerlike protrusions in wt (arrowheads) and the stubby and closely abutting toe-like protrusions in *α/β$_H$-spectrin* mutant (arrows). n, nucleus. For each genotype, 10 fusogenic synapses were analyzed with similar results. Scale bars, 500 nm. (i) Biochemical interaction between β$_H$-Spec and Duf. Co-immunoprecipitation (IP) experiment using extracts from embryos expressing Flag-β$_H$-Spec and Duf-GFP in muscle cells with *twi-GAL4*. Duf was pulled down with anti-Flag, but not a control antibody (anti-V5), suggesting interactions between β$_H$-Spec and Duf. α-Spec was probed to indicate the presence of β$_H$-Spec, the latter of which was difficult to detect due to its large size (~480 kD). These experiments were repeated three times with similar results. Unprocessed original scans of blots in Supplementary Fig. 5a.

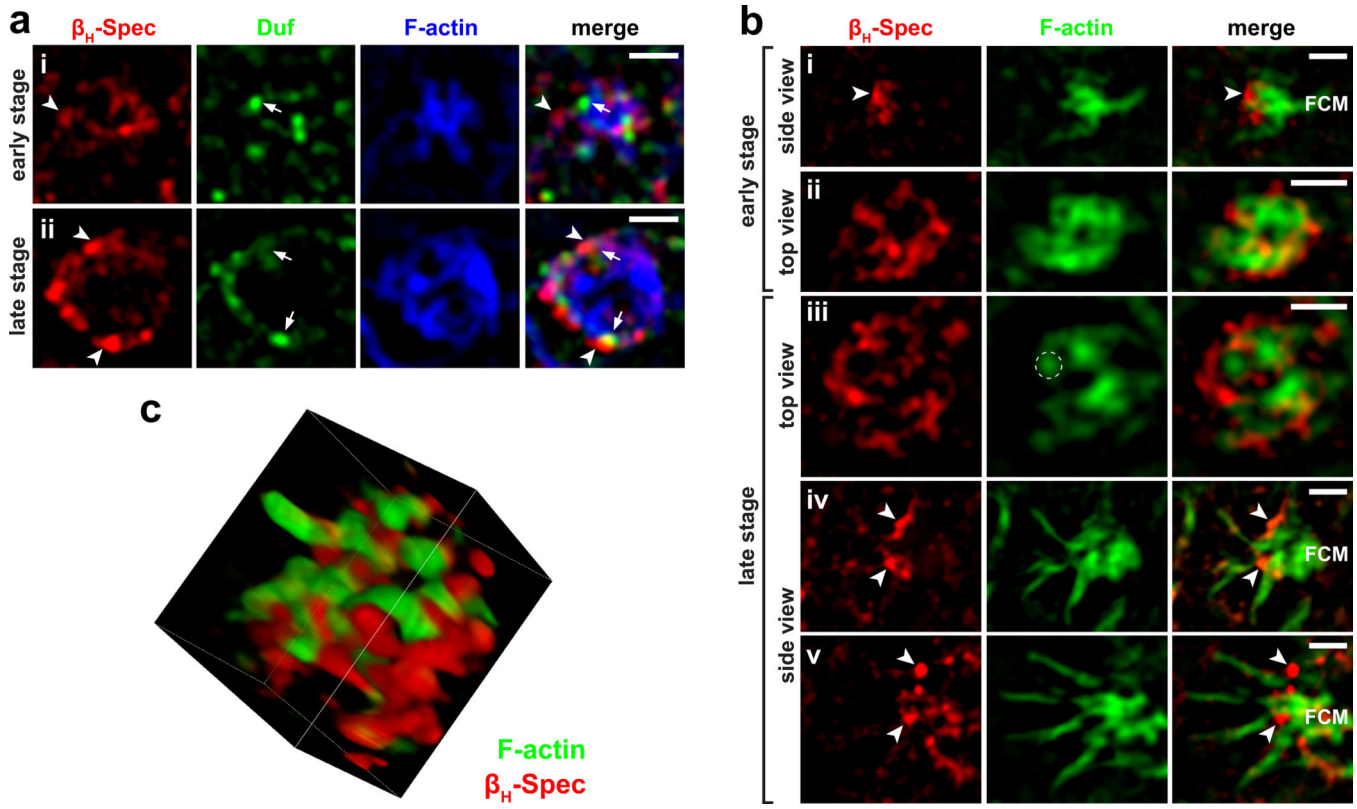

Figure 6. The α/β_H-spectrin network restricts the cell adhesion molecule Duf and constricts actin-propelled invasive protrusions

SIM images of fusogenic synapses in stage 14 embryos of a *β_H-spec* trap line. In (a) and "top view" panels in (b), the imaging plane was perpendicular to the axis of FCM invasion. In the "side view" panels in (b), the imaging plane was parallel to the axis of FCM invasion. (a) The α/β_H-spectrin network restricts Duf. An early stage (i) and a late stage (ii) fusogenic synapse labeled with β_H-Spec (red), Duf (green) and phalloidin (blue). Note the distinct microdomains occupied by β_H-Spec (arrowhead) and Duf (arrow) at the early stage (i), and the ring-like structure formed by β_H-Spec and Duf at the late stage, where these two proteins were closely associated with each other (ii). Also note that β_H-Spec was localized at the outer rim of the ring structure that kept most of the Duf clusters inside (ii). 25 fusogenic synapses were imaged with similar results. Scale bars, 1 μm. (b) The α/β_H-spectrin network constricts invasive protrusions. Side view (i, iv, v; FCM on the right) and top view (ii, iii) of early stage (i, ii) and late stage (iii-v) fusogenic synapses, labeled with β_H-Spec (red) and F-actin (green). (i) Accumulated β_H-Spec (arrowhead) locally blocked protrusions shown on this focal plane. (ii, iii) Actin-propelled protrusions triggered β_H-Spec accumulation at the base areas. These protrusions appeared wider at the early stage (ii) than the late stage (iii). Dashed circle outlines the cross section of a narrow protrusion (iii). (iv, v) Two examples of late stage fusogenic synapses, showing spectrin-enriched patches (arrowheads) blocking protrusions, as well as long and narrow protrusions from the FCM penetrating through spectrin-free microdomains. Note that these protrusions triggered further accumulation of β_H-Spec at their tips and/or sides. 40 fusogenic synapses were imaged with similar results. Scale bars, 1 μm. (c) 3D reconstruction of the fusogenic synapse shown in (b*iii*). Note the

actin-propelled protrusions penetrating through spectrin-free microdomains. 10 fusogenic synapses were reconstructed with similar results.

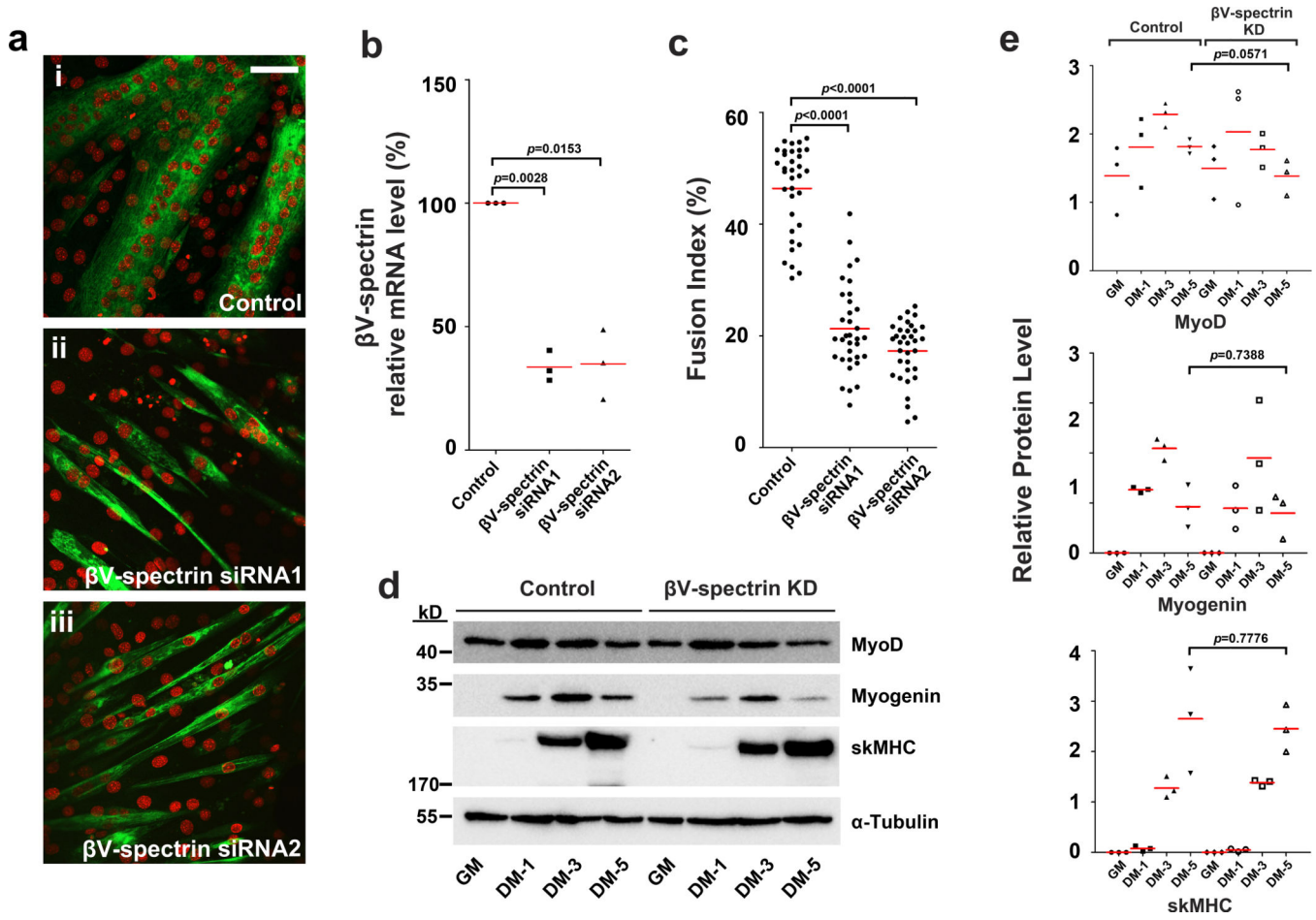

Figure 7. βV-spectrin, the mammalian homologue of *Drosophila* β_H-spectrin, is required for C2C12 myoblast fusion

(a) Confocal images of C2C12 cells treated with either transfection reagent alone (i) or two individual siRNAs against βV-spectrin (ii, iii). Cells were fixed on day 6 post differentiation and stained with anti-MHC (green) and DAPI (red) to visualize differentiated muscle cells. Note the thinner myofibers in (ii, iii) compared with (i). These experiments were repeated three times with similar results. Scale bar, 50 μm. (b) siRNA knockdown (KD) of βV-spectrin analyzed by qRT-PCR. The mRNA level of βV-spectrin in KD cells was normalized against control in n=3 independent experiments. (c) The fusion index was calculated as the percentage of nuclei in multinucleated syncytia versus the total number of nuclei per microscopic field. Each data point represents the fusion index of a random 20X microscopic fields; n=34 fields pooled from three independent C2C12 cell differentiation experiments. Note that βV-spectrin KD significantly decreased the fusion index. (d, e) βV-spectrin KD did not inhibit myoblast differentiation. (d) Western blot analyses showed no significant difference in the expression levels of myogenic differentiation markers (MyoD, Myogenin, and skeletal muscle MHC (skMHC)) between control and βV-spectrin KD cells. The cell lysates used for SDS-PAGE were derived from the same experiment and the gels/blots were processed in parallel. α-tubulin was used as a loading control. Unprocessed original scans of blots in Supplementary Fig. 5b. (e) Quantification of protein expression in (d). Y axes in the graphs indicate the measured band intensity ratio of each protein relative to the loading

control (α-tubulin). n=3 independent experiments. Each data point represents the relative protein expression level measured in a single experiment. In (b, c, e), horizontal bar indicates mean value, and statistical significance was determined by the two-tailed Student's *t*-test (*p* values marked at the top).